

Aus dem Institut für Biosynthese neuraler Strukturen
des Zentrums für Molekulare Neurobiologie Hamburg
des Universitätsklinikum Hamburg-Eppendorf
Direktorin: Frau Prof. Dr. Melitta Schachner

**Stereological Analysis of the Motor Cortex and the Hippocampus
of Dermatan-4O-sulfotransferase1
(Chondroitin Sulfotransferase 14) knockout mice**

Dissertation

zur Erlangung des Grades eines Doktors der Medizin

dem Fachbereich Medizin der Universität Hamburg vorgelegt von

Ewa Helena Laczynska

aus Danzig

Hamburg 2011

Angenommen vom Fachbereich Medizin der Universität Hamburg am: 04.08.2011

Veröffentlicht mit Genehmigung der Medizinischen Fakultät der Universität Hamburg

Prüfungsausschuss, die Vorsitzende: Prof. Dr. M. Schachner

Prüfungsausschuss, zweiter Gutachter: PD Dr. A. Irintchev

Prüfungsausschuss, dritter Gutachter: Prof. Dr. M. Glatzel

CONTENTS

1. INTRODUCTION	1
1.1. Dermatan sulfate.....	1
1.2. HNK-1 sulfotransferase family	4
1.3. Dermatan-4-O-sulfotransferase1	7
1.4. Clinical manifestation of Chst14 deficiency	10
2. RATIONALE AND AIMS OF THE STUDY	12
3. MATERIAL AND METHODS	13
3.1. Animals.....	13
3.2. Preparation of tissue for sectioning	13
3.3. Preparation of cryostat sections.....	14
3.4. Analysis of gross anatomical variables	15
3.4.1. Organ weight	15
3.4.2. Cortical thickness	15
3.4.3. Hippocampus.....	16
3.5. Stereological analysis of immunohistochemically defined cell types	16
3.5.1. Antibodies.....	16
3.5.2. Immunohistochemical stainings	18
3.5.3. Stereological analysis	19
3.5.4. Light microscopic analysis of perisomatic puncta and pyramidal cell size	20
3.5.5. Photographic documentation	21
3.5.6. Statistical analysis	21
4. RESULTS.....	22
4.1. Morphometric analysis of gross-anatomical variables	22
4.1.1. Body and organ masses	22
4.1.2. Cortical thickness	23
4.1.3. Areas of the hippocampus	23
4.2. Immunohistochemical markers, quality of staining and qualitative observations in Chst14 +/- and Chst14 -/- animals.....	27
4.3. Stereological analysis of the motor cortex	29
4.3.1. General observations	29

CONTENTS

4.3.2. Total cell density	29
4.3.3. Total neuronal population.....	30
4.3.4. Interneurons	30
4.3.5. Glial cells.....	32
4.3.6. Microglia	33
4.4. Stereological analysis of the hippocampus.....	34
4.4.1. Principal cell density	34
4.4.2. Interneurons	35
4.4.3. Glial cells.....	38
4.5. Analyses of soma size and synaptic coverage of principal neurons in CA1 and CA3 hippocampal subfields	39
4.5.1. Synaptic coverage.....	39
5. DISCUSSION.....	42
5.1. Morphological aberrations in Chst14 -/- mouse.....	44
5.1.1. Gross morphological variables	44
5.1.2. Cell populations affected by the mutation in the Chst14 gene	45
5.1.3. Synaptic coverage of pyramidal neurons in the hippocampus	47
5.1.4. Cell populations unaffected by the mutation in the Chst14 gene	47
5.2. Possible functional significance of the structural aberrations in Chst14 deficient mice	48
5.3. Conclusion.....	50
6. SUMMARY	51
7. REFERENCES	53
8. ABBREVIATIONS.....	62
9. DANKSAGUNG	65
10. CURRICULUM VITAE	66
11. EIDESSTATTLICHE VERSICHERUNG	67

1. INTRODUCTION

The extracellular matrix (ECM) is crucial for the maintenance of tissue structural integrity and communication between cells in multicellular organisms. It is present in all tissues with variations in the relative amounts of different matrix molecules. The main components of the ECM are proteoglycans (PGs), proteins with covalently attached glycosaminoglycan (GAG) polysaccharide side chains, fibrous proteins (e.g. collagens and elastin), adhesive glycoproteins (e.g. fibronectin, laminin and tenascin-C), a variety of secreted growth factors, and other molecules. In the central nervous system (CNS), the ECM shows a unique composition and organization as it contains relatively small amounts of fibrous proteins and high amounts of GAGs and is organized around certain neurons to produce specialized condensed ECM, known as perineuronal nets. GAGs are either covalently bound to proteins as proteoglycans (PGs) or unbound in the form of hyaluronan and consist of unbranched polysaccharide chains composed of repeating disaccharide units. According to their sugar composition, the protein bound GAGs are classified as keratan sulfate (KS), chondroitin sulfate (CS), dermatan sulfate (DS), and heparan sulfate (HS). These oligosaccharide moieties on PGs are frequently and selectively modified with sulfate. As sulfation is temporally and spatially regulated, this indicates that the presence of sulfate in many cases confers biological function to these saccharides (Hooper et al. 1996; Bowman and Bertozzi 1999).

1.1. Dermatan sulfate

DS is the predominant GAG in the skin and it shows a widespread distribution in many other mammalian tissues (Rosenberg et al. 1985). It corresponds to a stereoisomeric form of chondroitin sulfate called chondroitin sulfate B (CS B). Chondroitin consists of repeating units of $(\text{GlcUA}\beta 1,3\text{GalNAc}\beta 1,4)_n$ and can undergo extensive modification by sulfation at the 4-hydroxyl, 6-hydroxyl or both 4- and 6-hydroxyls of N-acetylgalactosamine (GalNAc) and at the 2- or 3-hydroxyl of glucuronic acid (GlcUA). The variations in the sulfation pattern of chondroitin define the different subtypes of CS, described in Table 1.

1. INTRODUCTION

Chondroitin sulfate type	Systematic name	Site of sulfation
A	chondroitin-4-sulfate	carbon 4 of GalNAc sugar
C	chondroitin-6-sulfate	carbon 6 of the GalNAc sugar
D	chondroitin-2,6-sulfate	carbon 2 of the GlcUA and 6 of the GalNAc sugar
E	chondroitin-4,6-sulfate	carbons 4 and 6 of the GalNAc sugar

Table 1: Sulfation patterns of chondroitin sulfate types.

Variable units of GlcUA in CS are converted to iduronic acid (IdoUA) by glucuronyl-C5-epimerase to produce DS (Fig. 1) (for reviews see Fransson et al. 2000; Habuchi et al. 2000; Silbert and Sugumaran 2002a). Two epimerases, DS-epimerase 1 (Maccarana et al. 2006) and DS-epimerase 2 (Pacheco et al. 2009a), have been described. Therefore, *in vivo* DS bearing PGs mostly contain CS/DS hybrids. In addition to sulfation of the GalNAc on the C-4 hydroxyl, the GalNAc in dermatan can also be sulfated at the C-6 hydroxyl (Nadanaka et al. 1999), and the IdoUA can be sulfated at the C-2 hydroxyl (Cheng et al. 1994).

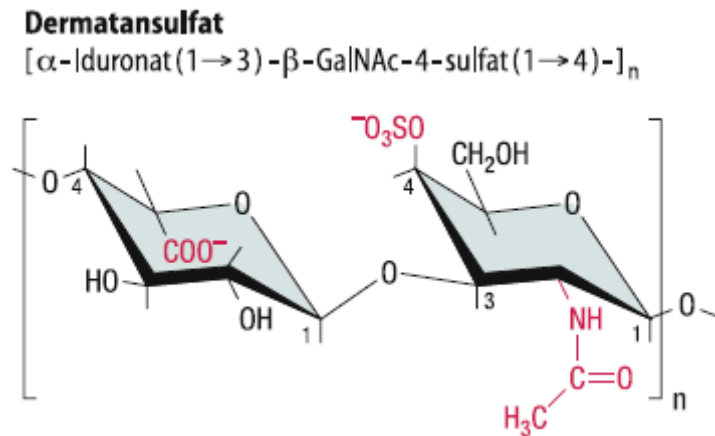


Figure 1: Structure of dermatan sulfate. Dermatan sulfate consists of (IdoUA β 1,3GalNAc β 1,4) $_n$ and (GlcUA β 1,3GalNAc β 1,4) $_n$ disaccharides (Löffler et al. 2007).

The level of complexity of DS-containing PGs and the DS sequence are affected by a diverse range of variables. Chain length, placement of IdoA, multiple alternatives for core proteins, sulfation and expression through the PG core protein in specific developmental and physiologic conditions are some of these variables (Bernfield et al. 1990; Kim et al. 1994). The family of CS/DS carrying proteoglycans includes versican, decorin, and biglycan. Decorin and biglycan are small PGs with one or two CS/DS chains, while versican is a large PG carrying multiple CS/DS chains (Iozzo 1998). There is a considerable variation of the proportion of IdoUA and GlcUA in CS/DS chains in tissues that is influenced by the level of free sulfate in the medium of cultured cells (Silbert et al. 1986). Cheng et al. (1994) showed that DS-type GAG chains are expressed in the brain as CS/DS hybrid chains with a larger proportion of GlcUA and a smaller proportion of IdoUA, in contrast to typical skin DS chains with a high content of IdoUA.

DS chains are important for many biological processes (for reviews see Trowbridge and Gallo 2002; Silbert and Sugumaran 2002b; Sugahara et al. 2003) including cell adhesion and migration (Kinsella et al. 1986), cell proliferation and recognition (Yamaguchi et al. 1990; Lyon et al. 1998), anti-coagulation process (Liaw et al. 2001; Fernandez et al. 1999; Iozzo 1998), wound healing, inflammation, and tumorigenesis (Trowbridge et al. 2002; Penc et al. 1998). In infections, DS chains are targets for bacterial, viral, and parasitic virulence factors for attachment, invasion, and immune system evasion (Rostand and Esko 1997; Schmidtchen

1. INTRODUCTION

et al. 2001). They are also stabilizers, cofactors, and/or coreceptors for growth factors, cytokines, and chemokines (Penc et al. 1999).

DS chains are also important for neural development as they influence neuronal adhesion, migration, and neurite formation (Bovolenta and Fernaund-Espinosa 2000; Sugahara et al. 2003; Lafont et al. 1992; Bandtlow and Zimmermann 2000; Sugahara and Kitagawa 2000). CS/DS chains, purified from embryonic pig brains (Bao et al. 2005) and neonatal mouse brains (Hikino et al. 2003), exhibit neurite outgrowth-promoting activity toward primary mouse hippocampal neurons *in vitro*. Bao et al. (2004) showed that these functions of CS/DS hybrid chains depend on their IdoUA content, which is higher in embryonic pig brain than in adult pig brain. Recent studies have shown that the ratios of GlcUA/IdoUA and GlcUA/GalNAc disaccharide units change during development of the chick, mouse, and pig brain (Mitsunaga et al. 2006). This shows that CS/DS chains differing in the degree and profile of sulfation may be involved in the specification of the functional diversity of neurons during brain development. However, the mechanism underlying the neuritogenic activity of CS/DS chains is not understood.

1.2. HNK-1 sulfotransferase family

The HNK-1 (Human natural killer cell antigen-1) sulfotransferase (ST) family is named after the HNK-1 carbohydrate structure, a sulfated glucuronyl-lactosaminyl residue carried by many neural recognition molecules. This carbohydrate was first recognized by a monoclonal antibody raised against human natural killer cells (Abo and Balch 1981). Many monoclonal antibodies have been described to bind to this carbohydrate epitope, each of which has slightly different HNK-1 binding properties. Interestingly, some HNK-1 antibodies require the presence of the sulfate group on the glucuronic acid, while others do not critically depend on it (Schmitz et al. 1994).

Based on sequence homology of Golgi-associated sulfotransferases and HNK-1 sulfotransferase (HNK-1ST or chondroitin sulfotransferase 10, Chst10), the consensus sequence xxRPDzzzx was discovered. Using this conserved sequence in HNK-1ST as a probe, Hiraoka et al. (2000) identified two expressed sequence tags in EST data base, which have 31.6% and 30.7% identity with HNK-1ST at the amino acid levels (Fig. 2). According to their function they called these enzymes chondroitin-4O-sulfotransferase 1 (C4ST1, Chst11) and chondroitin-4O-sulfotransferase 2 (C4ST2, Chst12).

1. INTRODUCTION

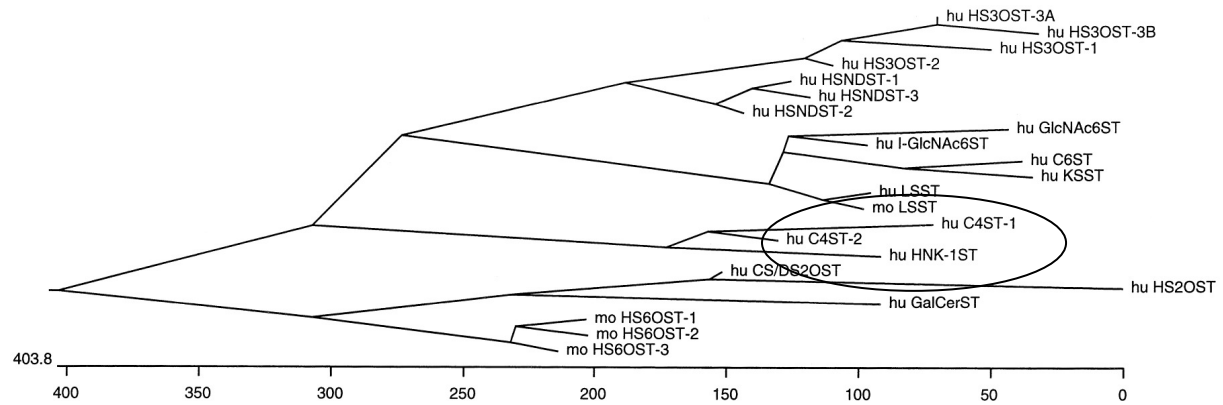


Figure 2: Schematic representation of the phylogenetic tree of Golgi-associated carbohydrate sulfotransferases. Amino acid sequences predicted from cloned cDNAs are compared using the ClustalW method with PAM250 residue weight table. Encircled are human HNK-1 sulfotransferase, hu HNK-1ST; Human chondroitin N-acetylgalactosamin-4O-sulfotransferase-1, -2, hu C4ST1,-2 (Hiraoka et al. 2000)

As a result of the homology to HNK-1ST, four more members of the so called HNK-1 sulfotransferase family were cloned, namely, N-acetylgalactosamine-4O-sulfotransferase 1 (GalNAc4ST1, Chst8; Xia et al. 2000; Hiraoka et al. 2001), N-acetylgalactosamine-4O-sulfotransferase 2 (GalNAc4ST2, Chst9; Kang et al. 2001; Hiraoka et al. 2001), dermatan-4O-sulfotransferase1 (D4ST1, Chst14; Evers et al. 2001) and chondroitin-4O-sulfotransferase 3 (Chst13, C4ST3; Kang et al. 2002). Each member of the HNK-1ST family has a short N-terminal cytosolic domain, a transmembrane domain (TM), followed by a stem region and the sulfotransferase domain, which consists of a 5'-phosphosulfonate binding site (5'-PSB), a 3'-phosphate binding site (3'-PB), and three regions of unknown function. These regions are called III, IV and V and they are carboxyl-terminal to the 3'-PB. The regions 5'-PSB, 3'-PB, and III, IV, and V show the highest percentages of identical amino acids and therefore they show a high degree of identity within the sulfotransferase domain (Fig. 3). These regions are characteristic for the HNK-1ST family but their functional significance remains to be elucidated. The stem region, the TM, and the cytosolic domain are the regions with the lowest percentage of identical amino acids among the HNK-1ST family members (Baenziger 2003).

1. INTRODUCTION

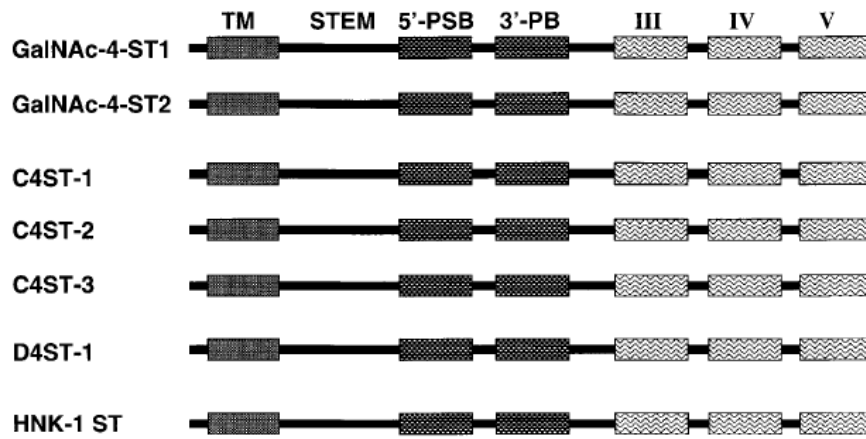


Figure 3: Overview over the HNK-1ST family protein structure. Each of the members has a short N-terminal cytosolic domain, a TM, followed by a stem region and the sulfotransferase domain with a 5'-PSB and 3'-PB, and the regions called III, IV and V (Baenziger 2003).

With the exception of the HNK-1ST, which transfers sulfate to the hydroxyl group of the third C-atom of terminal $\beta 1,3$ glucuronic acid, each of the other members sulfates the hydroxyl group of the fourth C-atom of either terminal or non-terminal $\beta 1,4$ linked N-acetylgalactosamine. PAPS (3'-phosphoadenosine 5'-phosphosulfate) serves them as a high energy sulfate donor for this transfer (Fukuda et al. 2001; Ong et al. 1999; Fig. 4).

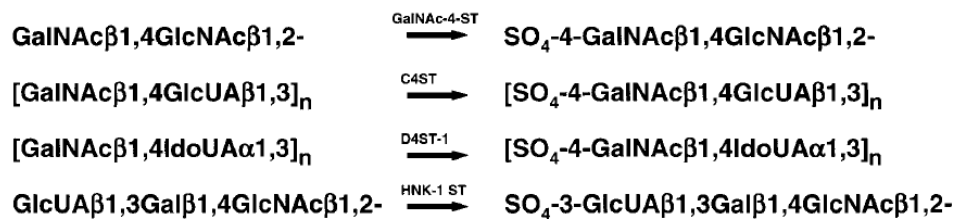


Figure 4: Epitopes of the different sulfotransferases. GalNAc4ST sulfates the hydroxyl group of the fourth C-atom of terminal, C4ST und D4ST1 sulfate non-terminal GalNAc in chondroitin/dermatan-GAG. HNK-1ST sulfates the third C-atom of terminal glucuronic acid (Baenziger 2003).

A study on the tissue distribution of the HNK-1ST family members in the mouse has recently shown that all members have overlapping expression patterns in most mouse tissues. Importantly, all HNK-1ST family members are highly expressed in the adult mouse brain (Hoffmann 2007).

1.3. Dermatan-4O-sulfotransferase1

The dermatan specific N-acetylgalactosamine-4O-sulfotransferase (designated D4ST1 or Chst14) was cloned in 2001 (Evers et al. 2001). It transfers sulfate to the C-4 hydroxyl of β 1,4-linked GalNAc that is substituted with an β -linked IdoUA at the C-3 hydroxyl and is only active on dermatan-type structures. In their studies on the acceptor specificity of Chst14, Evers et al. (2001) and Mikami et al. (2003) have reached different conclusions. Evers et al. (2001) find that Chst14 has a strong preference for IdoUA-GalNAc flanked by GlcUA-GalNAc, but not for IdoUA-GalNAc flanked by IdoUA-GalNAc, while Mikami et al. (2003) provide evidence that Chst14 far more efficiently transfers sulfate to GalNAc residues in IdoUA-GalNAc-IdoUA than in –GlcUA-GalNAc-GlcUA (Fig. 5).

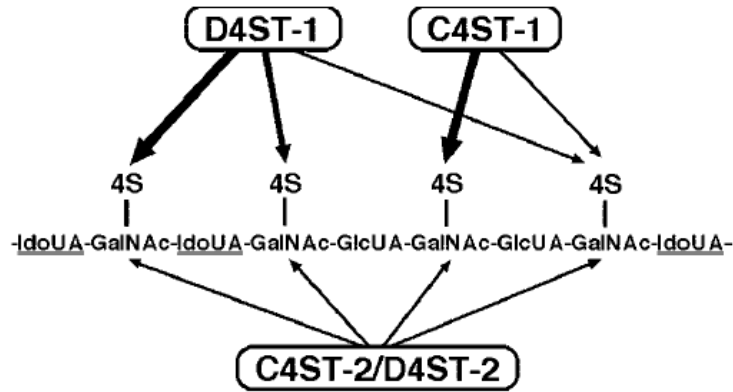


Figure 5: Schematic representation of the substrate specificities of D4ST1 (Chst14), C4ST1, and C4ST2/D4ST2 toward a CS/DS polysaccharide backbone. Arrows are indicating potential sulfation sites in the schematic repeating disaccharide sequence of a CS/DS hybrid structure catalyzed by D4ST1 (Chst14), C4ST1, and C4ST2/ D4ST2. The thickness of each arrow shows the relative preference of each enzyme for IdoUA-GalNAc-IdoUA-, -IdoUA-GalNAc-GlcUA-, and -GlcUA-GalNAc-IdoUA-. Possible effects of sulfate groups on the depicted sulfation reactions are not considered here and the activity of C4ST1 toward the -GlcUA-GalNAc-IdoUA- sequence has been reported in Habuchi 2000 (Mikami et al. 2003).

Furthermore, Evers et al. (2001) describe that sulfation of GalNAc in dermatan is immediately followed by the epimerization of GlcUA to IdoUA as D4ST1 selectively sulfates IdoUA-GalNAc that is flanked by GlcUA-GalNAc, thereby consequently protecting it from the back epimerization as discussed before for the reactions of the recombinant D4ST1 (Malmström 1984). In contrast, Mikami et al. (2003) show that C5 epimerization precedes 4-O-sulfation and furthermore 4-O-sulfation promotes subsequent 4-O-sulfation of GalNAc in the neighboring disaccharide unit. 4-O-sulfated IdoA blocks are of particular importance for the biological functions of dermatan sulfate. They bind to ligands such as fibroblast growth factor 2, hepatocyte growth factor, and heparin cofactor II (Maimone and Tollefsen 1990; Lyon et al. 1998; Taylor et al. 2005). In their recent study, Pacheco et al. (2009b) show that loss of D4ST1 leads to a substantial reduction in IdoA residues located in block structures without affecting the epimerase activity. Furthermore, the observation that aberrant 4-O-sulfation of GalNAc indicates that C4ST1 and C4ST2 are not able to compensate the function of D4ST1. These results emphasize that D4ST1 has a pivotal role in the biosynthesis and function of DS.

1. INTRODUCTION

The Chst14 locus is found on the human chromosome 15q4 and appears to be encoded by a single exon. The Chst14 cDNA predicts an open reading frame encoding a type II membrane protein of 376 amino acids with a 43-amino acid cytoplasmic domain and a 316-amino acid luminal domain containing two potential N-linked glycosylation sites and PAPS binding motifs. The human Chst14 has significant amino acid identity with Chst10 (21.4%), Chst8 (24.7%), Chst9 (21.0%), Chst11 (27.3%), and Chst12 (22.8%) (Evers et al. 2001). Evers et al. (2001) use Northern blot transcript and array analyses to determine the expression pattern for Chst14 in human tissues. The array analysis has indicated that most tissues express at least modest levels of the D4ST1 message. The strongest signals are seen in pituitary, placenta, uterus, thyroid, fetal lung, and the colorectal adenocarcinoma cell line SW480. Whereas Northern Blot analysis has revealed single 2,4-kilobase in heart, placenta, liver, and pancreas and significantly lower levels in skeletal muscle and kidney (Fig. 6). These results show that the expression levels of Chst14 message in different tissues is largely variable.

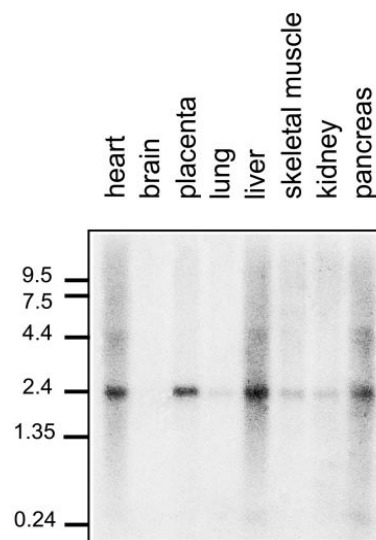


Figure 6: Northern blot analysis of Chst14 transcripts. Each lane of the MTN® Northern blot contains 2 g poly (A) RNA and was hybridized with a ³²P-labeled cDNA probe specific for human Chst14. Tissues used to prepare the RNA are indicated above each one (Evers et al. 2001).

1.4. Clinical manifestation of Chst14 deficiency

Congenital disorders of glycosylation are known from all medical subspecialties. This group includes all genetic diseases that result from defects in the synthesis of glycans. Just recently, two new manifestations were discovered. They represent a new class as their defect is specifically connected to DS biosynthesis, even more precisely to dysfunction of Chst14.

Dündar et al. (2009) showed that Chst14 is the causative gene for autosomal recessive adducted thumb-clubfoot syndrome (ATCS). This syndrome has been categorized as a new type of arthrogryposis. The clinical picture is characterized by adducted thumb and clubfoot as well as craniofacial dysmorphism, arachnodactyly with tapering fingers, cryptorchidism, inguinal hernia, atrial septal defect, kidney defects, cranial ventricular enlargement, and psychomotor retardation (Dündar et al. 1997, 2001; Janecke et al. 2001; Sonoda and Kouno 2000). Dündar et al. (2009) categorized ATCS as a connective tissue disorder. This observation is based on additional clinical pictures from childhood to adolescence. It includes skin fragility, bruisability, and translucency, furthermore joint laxity and osteopenia. The patients with ATCS were found to have severe manifestations as four out of 11 patients identified died in early infancy or childhood. These findings suggest not only an implication of Chst14 in the connective tissue maintenance but also in embryonic development (Dündar et al. 2009).

Miyake et al. (2010) discovered another Chst14 mutation relevant for the Ehlers-Danlos syndrome (EDS). The EDS is a clinically and genetically heterogeneous connective tissue disorder, which affects 1 in 5000 individuals. It is manifested by skin hyperextensibility, joint laxity and generalized connective tissue fragility (Steinmann et al. 2002). In a revised nomenclature proposed by Beighton et al. (1998), EDS has been classified into six subtypes. EDS kyphoscoliosis type (EDS Typ VIA and VIB) is an autosomal recessive disorder. It is characterized by early-onset progressive kyphoscoliosis, severe neonatal muscle hypotonia with delayed gross motor development, generalized joint hyperlaxity, marfanoid habitus, osteopenia, and a fragile, hyperextensible, and bruisable skin with widened atrophic scars. In some cases, scleral fragility with risk for rupture of the globe, and life threatening rupture of medium-sized arteries have been reported (Yeowell and Steinmann 2000). Craniofacial abnormalities, joint contractures, wrinkled palms, and normal levels of lysyl hydroxylase-1 activity distinguish EDS VIB from EDS VIA (Kosho et al. 2005, 2010; Steinmann et al. 1975,

1. INTRODUCTION

2002; Walker et al. 2004). Miyake et al. (2010) investigated EDS type VIB and identified a homozygous Chst14 mutation in two familial cases and compound heterozygous mutations in four sporadic cases. Most interestingly, the DS of the decorin proteoglycan, which is known to regulate collagen fibril assembly, is completely replaced by CS in these cases. These findings showed a novel pathological mechanism in EDS and the importance of DS in the extracellular matrix.

Recently, Malfait et al. (2010) identified, using a genome wide single nucleotide polymorphism (SNP) scan and sequence analysis, an identical mutation in patients with EDS type VIB and ATCS. This suggests that both conditions form a phenotypic continuum and therefore represent a single clinical entity caused by mutations in Chst14 gene. They call this entity “musculocontractural EDS”.

2. RATIONALE AND AIMS OF THE STUDY

Previous work has shown the importance of CS/DS GAGs in development and regeneration of the CNS structures. However, in all previous studies it was difficult to functionally distinguish between various CS/DS forms. To this end, mice deficient in Chst14, the key enzyme indispensable for the formation of iduronic acid - containing blocks in DS were created in the laboratory of Professor Melitta Schachner. The aim of my study was to characterize Chst14 deficient (Chst14 $-/-$) mice with regard to anatomy and histology of two commonly studied brain regions – the motor cortex and the hippocampus. The motor cortex is known to be involved in the planning, control, and execution of voluntary motor functions. The hippocampus belongs to the limbic system and plays major roles in short-term memory and spatial navigation. The study of the 2-month-old Chst14 $-/-$ mice, in comparison with wild-type (Chst14 $+/+$) littermates is designed to uncover large, as well as subtle morphological differences between the genotypes, and thus clarify the role of DSs in development of these functionally important structures.

This study addressed the following questions:

- Does Chst14 deficiency cause gross-anatomical abnormalities such as changes of the total brain weight and volume, neocortical thickness, and size of the hippocampus?
- Are there alterations in the size of major neuronal and glial cell populations in Chst14 $-/-$ mice?
- Are there changes in the number of inhibitory synaptic terminals on the pyramidal cell bodies in the hippocampus caused by Chst14 deletion?

These questions were addressed using quantitative methodology, established by Irintchev et al. (2005), which is based on immunohistochemical visualization of defined cell types and stereological estimation of cell densities.

3. MATERIAL AND METHODS

3.1. Animals

Wild-type (Chst14 +/+) mice and Chst14-deficient (Chst14 -/-) littermates were studied at the age of 2 months (N = 6 per genotype). The animals were bred in the pathogen-free facility of the Universitätsklinikum Hamburg-Eppendorf. The delivery to the Institute was on the day of sacrifice and all animals appeared healthy upon arrival. The genotype of the mutant mice had been determined in advance by polymerase chain reaction (PCR) assay and Southern Blot. All treatments of the animals were performed in accordance to the German law for protection of experimental animals. The technical procedures described below were performed according to Irintchev et al. (2005).

3.2. Preparation of tissue for sectioning

Mice were weighted and anesthetized with 16% weight/volume (w/v) solution of sodium pentobarbital (Narcoren, Merial, Hallbergmoos, 5 μ l g⁻¹ body weight, i.p.). After surgical tolerance was achieved, the animals were transcardially perfused with physiologic saline for 60 seconds followed by fixative consisting of 4% formaldehyde and 0.1% CaCl₂ in 0.1M cacodylate buffer, pH 7.3, for 15 minutes at room temperature (RT). Cacodylate buffer supplemented with calcium was selected for use in order to ensure optimal tissue fixation including preservation of highly soluble antigens like S-100 (Rickmann and Wolff 1995). Following perfusion, the brains were left *in situ* for 2 hours at RT to reduce fixation artifacts (Garman 1990). Subsequently, they were dissected out without the olfactory bulbs and post-fixed overnight (18-22 hours) at 4°C in the formaldehyde solution used for perfusion supplemented with 15% w/v sucrose. Tissue was then immersed into 15% sucrose solution in 0.1M cacodylate buffer, pH 7.3, at 4°C for two days.

Fixed and cryoprotected (sucrose-infiltrated) brains were carefully examined under a stereomicroscope and hair, rests of dura mater or other tissue debris were removed with a fine forceps. Following this, the brains were placed in a mouse brain matrix (World Precision Instruments, Berlin) and the caudal end was cut at a defined level (1 mm from the most caudal slot of the matrix). Then brain mass was measured (3.4.1). Finally, the brains were frozen by insertion for 2 minutes into 2-methyl-butane (isopentane), which had been precooled to -30°C in the cryostat. The brains were stored in liquid nitrogen until sectioned.

3.3. Preparation of cryostat sections

For sectioning, the caudal pole of each brain was attached to a cryostat specimen holder using a drop of distilled water placed on a pre-frozen layer of Tissue Tek (Sakura Finetek Europe, Zoeterwoude, The Netherlands). The ventral surface of the brain was oriented to face the cryostat knife edge and serial coronal sections of 25 µm thickness were cut in a cryostat Leica CM3050 (Leica Instruments, Nußloch, Germany). Sections were collected on SuperFrost Plus glass slides (Roth, Karlsruhe, Germany). Since stereological analyses require extensive sectioning of the structures studied and use of spaced-serial sections (Howard and Reed 1998), sampling was always done in a standard sequence so that 4 sections 250 µm apart were present on each slide (25 µm thick sections) (Fig. 7).

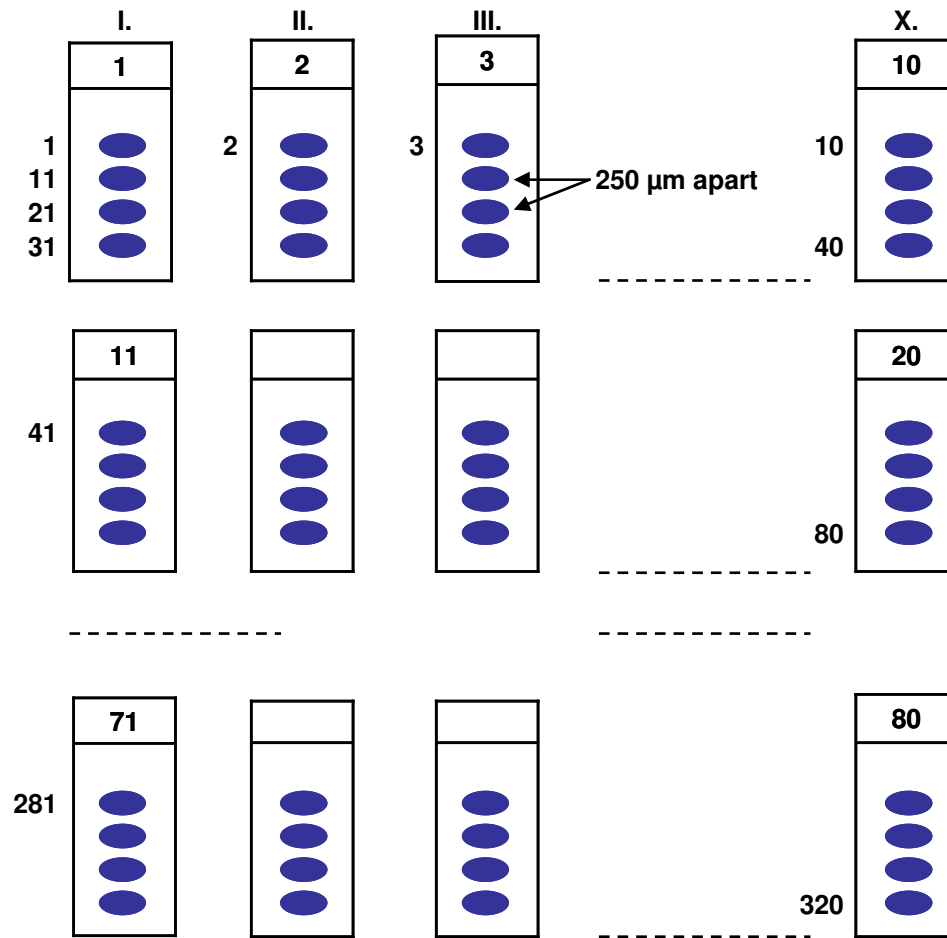


Figure 7: Standardized sequence of collecting sections (25µm) on glass slides. Staining of slides from one row (e.g., 1, 11, etc.) with a given antibody (see below) gives the opportunity to evaluate a cell population using randomly spaced samples from a brain structure of interest.

3.4. Analysis of gross anatomical variables

3.4.1. Organ weight

Brain, tibia, heart, liver, kidney, and spleen of each animal were dissected after perfusion fixation, blotted with filter paper to remove excess liquid from the surface and weighed using a fine 4-digit scale (BP61, Sartorius, Göttingen, Germany).

3.4.2. Cortical thickness

To determine the average cortical thickness in the motor cortical areas, 25 µm sections cut 3 to 4 mm caudally to the rostral pole stained with bis-benzimide to visualize nuclei were used.

3. MATERIAL AND METHODS

The nuclear staining allowed clear distinction of the agranular motor and the granular sensory cortex. The area of the motor cortical field and the length of its surface boundary were measured directly under the Axioskop microscope using the Neurolucida software (MicroBrightField Europe, Magdeburg, Germany). The mean cortical thickness was calculated by dividing the area by the length of the superficial boundary.

3.4.3. Hippocampus

The area of the whole hippocampal formation, and areas of the subfields (gyrus dentatus (DG), CA3 and CA1), principle cell layer (in DG, CA1 and CA3), stratum radiatum (in CA1 and CA3), stratum oriens (in CA1 and CA3), stratum lacunosum-moleculare (in CA1), stratum polymorphe (in DG), stratum moleculare (in DG) were measured bilaterally in every animal in three coronal sections with nuclear staining using the Neurolucida system. The criterion for the selection of the mid-section was similarity in appearance to that of section (bregma–2.1 mm) shown in the mouse brain atlas of Sidman et al. (1971). The other two sections were 250 µm apart from the mid-section, one rostral to it, one caudal. Since spacing between the evaluated sections was equal and relatively large (250 µm), the area estimates are proportional to the volume of a significant portion of the dorsal hippocampus. The average of three values per animals and area was used to calculate group mean values.

3.5. Stereological analysis of immunohistochemically defined cell types

3.5.1. Antibodies

The antibodies used in this study, summarized in Table 2, recognize specific cell-marker antigens known to be expressed in defined cell populations in the brain regions studied here (Irintchev et al. 2005):

3. MATERIAL AND METHODS

Antibody	Abbreviation	Clone	Producer	Dilution
Anti-Parvalbumin	Anti PV	mouse monoclonal, clone: Parv 19	Sigma, <i>Deisenhofen, Germany</i>	1:1000 9.8µg/ml Ig
Anti-Neuron specific nuclear antigen	Anti NeuN	mouse monoclonal, clone: A60	Sigma, <i>Deisenhofen, Germany</i>	1:1000 1µg/ml Ig
Anti-Cyclic nucleotide phosphatase	Anti CNPase	mouse monoclonal, clone: 11-5B	Sigma <i>Deisenhofen, Germany</i>	1:1000 7.5µg/ml Ig
Anti-S-100	Anti S-100	rabbit polyclonal, purified IgG fraction	DakoCytomation, <i>Hamburg, Germany</i>	1:500 9µg/ml Ig
Anti-Vesicular GABA transporter	VGAT	rabbit polyclonal, antibody	Synaptic Systems, <i>Göttingen, Germany</i>	1:1000 1µg/ml Ig
Anti-Reelin	Anti reelin	mouse monoclonal, clone: G10	Chemicon, <i>Hofheim, Germany</i>	1:500 2µg/ml Ig
Anti-Iba1	Anti Iba1	rabbit polyclonal, affinity purified	Wako Chemicals, <i>Neuss, Germany</i>	1:1500 0.3µg/ml Ig

Table 2: Commercially available antibodies that were used at optimal dilutions in this study. Shown are abbreviations, clones and producers of the antibodies and the optimal dilution of each antibody.

3. MATERIAL AND METHODS

- **PV** is a low molecular weight calcium-binding protein expressed in a major subpopulation of GABAergic neurons in the neocortex and hippocampus.
- **NeuN** is a protein of unknown function shown to be present in all neurons in the adult brain with the exception of a few cell types, which are not found in the cerebral cortex and hippocampus though (Purkinje, mitral and photoreceptor cells, Wolf et al. 1996).
- **CNPase** is an enzyme only present in cells which are able to synthesize myelin, i.e. oligodendrocytes and Schwann cells.
- **S-100** is a low molecular weight calcium-binding protein expressed in astrocytes.
- **VGAT** is a transporter, which mediates accumulation of inhibitory neurotransmitters GABA and glycine into synaptic vesicles. VGAT is highly concentrated in the nerve endings of GABAergic and glycinergic neurons in the brain and spinal cord (Chaudhry et al. 1998).
- **Reelin** identifies inhibitory interneurons (bitufted, horizontal and Martinotti cells), which do not express PV (Pesold et al. 1999).
- **Iba1** is a macrophage/microglia-specific calcium-binding protein involved in the activation of quiescent microglial cells (Imai and Kohsaka 2002).

3.5.2. Immunohistochemical stainings

The immunohistochemical stainings were performed as described by Irintchev et al. (2005). Sections, stored at -20°C, were air-dried for 30 minutes at 37°C. A 10mM sodium citrate solution (pH 9.0, adjusted with 0.1M NaOH) was prepared in a jar and preheated to 80°C in a water bath. The sections were incubated at 80°C for 30 minutes after which the jar was taken out and left to cool down to RT. After cooling down, blocking of unspecific binding sites was performed. The sections were incubated at RT for one hour in PBS containing 0.2% v/v (volume/volume) Triton X-100 (Fluka, Buchs, Germany), 0.02 w/v sodium azide (Merck, Darmstadt, Germany), and 5% v/v normal goat serum (Jackson Immuno Research Laboratories, Dianova, Hamburg, Germany). After one hour the blocking solution was aspirated and incubated with the primary antibody diluted in PBS containing 0.5% w/v lamda-carrageenan and 0.02% w/v sodium azide in PBS. The slides were incubated for 3 days at 4°C in a well sealed staining jar. Following this, the sections were washed 3 times in PBS (15 minutes each) before an appropriate (anti-rabbit or anti-mouse) secondary antibody was applied. The sections were incubated with the secondary antibody diluted (1:200) in PBS-carrageenan at RT for 2 hours. Goat anti-rabbit or goat anti mouse IgG conjugated with Cy3 (cyanine 3; Jackson Immuno Research Laboratories) was used. After a subsequent wash in

3. MATERIAL AND METHODS

PBS, cell nuclei were stained for 10 minutes at RT with bis-benzimide solution (Hoechst 33258 dye, 5µg/ml in PBS, Sigma, Deisenhofen, Germany). Finally, the sections were washed again, mounted with Fluoromount G (Southern Biotechnology Associates, Biozol, Eching, Germany) and stored in the dark at 4°C.

For a given antigen, all sections were stained in the same solution kept in screw-capped staining plastic jars (capacity 35 ml, 10 slides, Roth). Double staining for PV and VGAT was preformed by mixing the primary antibodies at optimal dilutions and using Cy3-conjugated anti-mouse and a Cy2-labeled anti rabbit secondary antibody pre-absorbed with rabbit and mouse serum proteins, respectively (multi-labeling grade antibodies, Jackson ImmunoResearch).

3.5.3. Stereological analysis

The cell counts were performed on an Axioskop microscope equipped with a motorized stage and NeuroLucida software controlled computer system (MicroBrightField). The agranular motor areas as well as the subdivisions of the hippocampus were identified at low magnification by viewing the nuclear staining (Plan-Neofluar_ 10x/0.3 objective). The viewed area was randomized by setting a reference point at an arbitrary place resulting in an overlay of the visible field by a grid with lines spaced 30µm (in the NeuN staining), 25µm (cell nuclei in the hippocampus), or 60µm (all other areas and stainings studied). The contours of the area of interest were outlined with the cursor. For the motor cortex, layer I was excluded from all measurements because parts of it were sometimes lost together with pieces of pia mater during cutting. Squares outlined by the projected grid within the marked area at distances of 30µm for the NeuN staining and 120µm for the other stainings were labeled and used as disectors for the three-dimensional counting. The disector depth was 10µm for all quantifications. The sections were viewed with the 40x magnification objective and 546/590nm excitation/emission filter set (15, Zeiss, red fluorescence). The marked area was meander scanned and all marked frames were viewed consecutively. Immunolabeled cell profiles that were entirely within the counting frame at any focus level, as well as those attaching to or intercrossed by the forbidden or acceptance lines were marked with a symbol. Then by repeated switching between the red and blue filter sets and changing the focus plane, the nuclei of the labeled cells were identified. All nuclei that were in focus beyond a guard space (depth 0-2µm from the section surface), i.e. lying within 2 and 12µm below the top of the section, were counted except those at the “look-up” level (2µm) and such intercrossed by

or touching the forbidden lines. Four sections were evaluated bilaterally per animal and staining.

3.5.4. Light microscopic analysis of perisomatic puncta and pyramidal cell size

Estimation of perisomatic puncta and area of principal cell bodies in the regions CA1 and CA3 of the hippocampus was performed as previously described (Irintchev et al. 2005; Nikonenko et al. 2006). Stacks of images of 1 μm thickness were obtained from sections double stained with PV and VGAT on a LSM 510 confocal microscope (Zeiss) using a 63x oil immersion objective and the digital resolution 1024 x 1024 pixels. One merged image (red and green channel) per cell at the level of the largest cell body cross-sectional area was used to measure soma perimeter and area and to count individually discernible perisomatic puncta (Fig. 8). The number of PV^+VGAT^+ and PV^-VGAT^+ puncta was counted and normalized to the perimeter of the cell measured using Image Tool 2.0 software (University of Texas Health Science Centre, San Antonio, Texas).

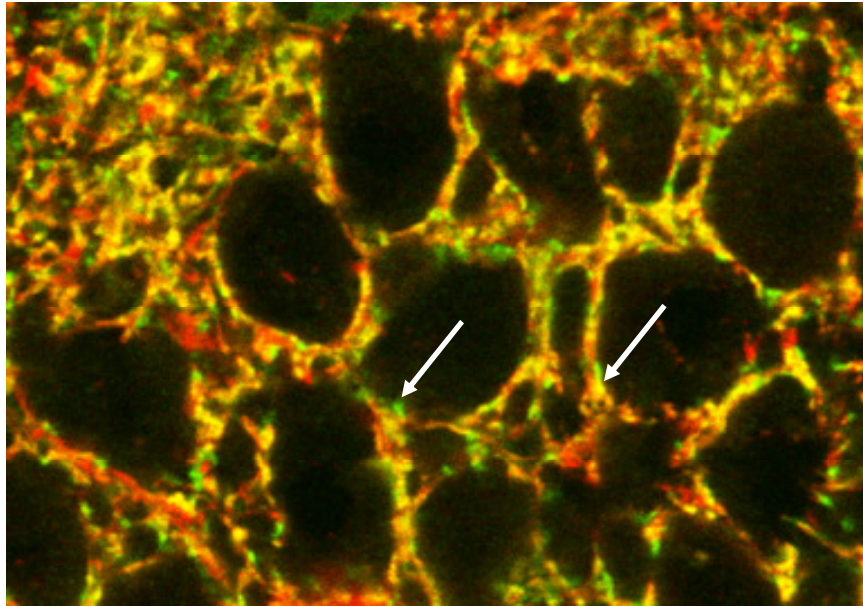


Figure 8: GABAergic synaptic coverage of pyramidal cells in the CA3 hippocampal fields in a Chst14 ^{-/-} mouse. Counted are GABA presynaptic terminals labeled with vesicular GABA transporter around the perimeter of pyramidal cells that are PV⁺ (yellow on the overlay image) or PV⁻ (green on the overlay image). The arrows point on examples of perisomatic puncta.

3.5.5. Photographic documentation

Photographic documentation was made on an Axiophot 2 microscope equipped with a digital camera AxioCam HRC and AxioVision software (Zeiss) at the highest resolution (2300x2300 pixel, RGB). The images were processed using Adobe Photoshop 6.0 software (Adobe Systems Inc., San Jose, California).

3.5.6. Statistical analysis

Group mean values were compared using SigmaStat 2.0 software (SPSS, Chicago, IL). Group mean values were compared using two-sided *t*-test for independent groups. By two or more measurements per parameter and animal, the mean was used as a representative value. Thus, for all comparisons the degree of freedom was determined by the number of animals. The accepted level of significance was 5%.

4. RESULTS

4.1. Morphometric analysis of gross-anatomical variables

4.1.1. Body and organ masses

The brain weight of 2-month-old Chst14 $-/-$ animals did not differ significantly from that of Chst14 $+/+$ animals, whereas the body weight showed a significant difference (Fig. 9). The average body weight was by 21% lower in mutant animals compared with wild-type mice, which can explain the significantly smaller mass of major organs in Chst14 $-/-$ compared with wild-type animals: tibia -41%, heart -37%, liver -34%, and kidney -29% (Fig. 9).

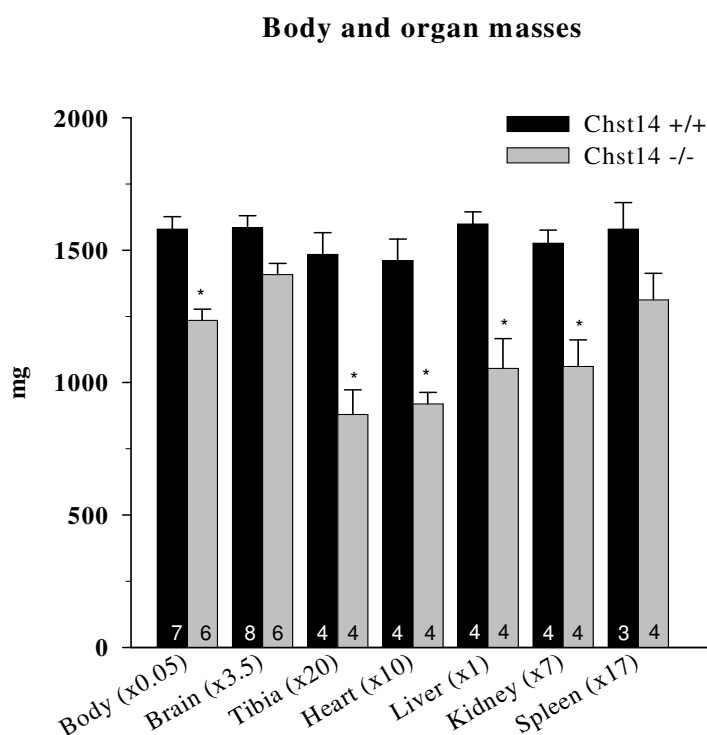


Figure 9: Body and organ masses (in mg) of Chst14 $+/+$ (black bars) and Chst14 $-/-$ animals (grey bars). Shown are mean values + standard errors of mean (SEM). The numbers in the bars indicate the number of animals per group. Asterisks indicate significant differences between the groups (two-sided t -test for independent groups, $p < 0.05$ t -test).

4. RESULTS

4.1.2. Cortical thickness

The normalized cortical thickness, calculated as ratio of the cortical segment area (excluding layer I) to the length of the surface (meningeal) boundary of the segment, was similar in the two genotypes (Fig. 10).

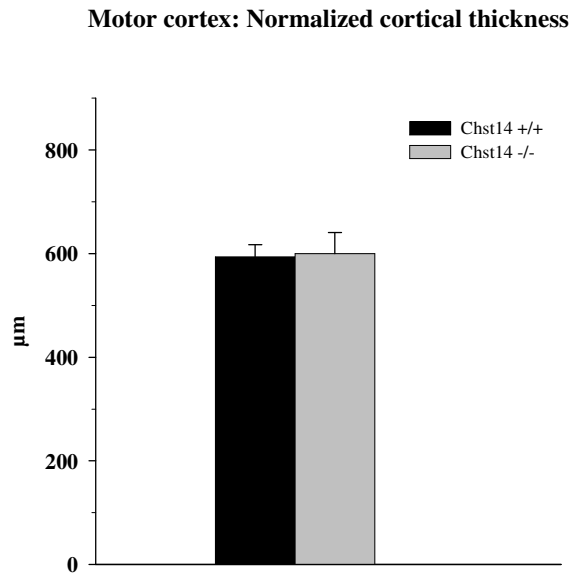


Figure 10: Normalized thickness of the motor cortex in Chst14 +/+ (black bar) and Chst14 -/- animals (grey bar). Shown are mean values + standard deviations (SD). No significant difference was found (*t*-test).

4.1.3. Areas of the hippocampus

The cross-sectional areas of the hippocampal subfields were measured in three spaced-serial sections (250 μm apart) from the dorsal hippocampus cut at defined levels (see 3.4.3.). Not only the total area of the hippocampus (Fig. 11) but also the subfield areas (CA1-CA3 and DG) of the hippocampus (Fig. 12) showed no significant difference between the genotypes.

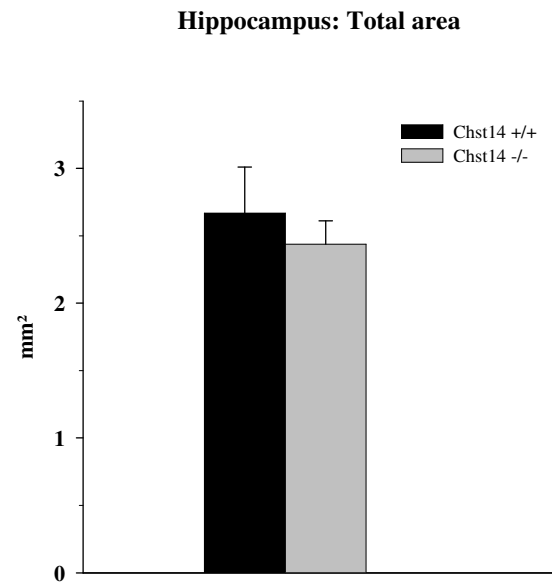


Figure 11: Total cross-sectional area of the hippocampus measured in coronal brain sections from Chst14 +/+ (black bar) and Chst14 -/- animals (grey bar). Shown are averaged bilateral mean values + SD. No significant difference was found (*t*-test).

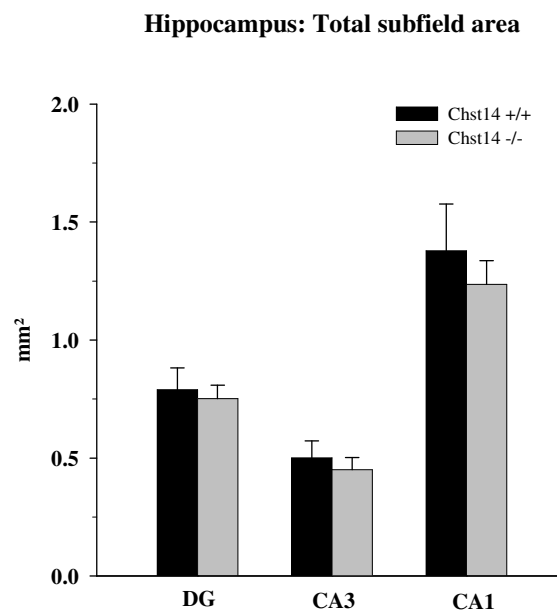


Figure 12: Total area of hippocampal subfields in coronal brain sections from Chst14 +/+ (black bars) and Chst14 -/- animals (grey bars). Shown are averaged bilateral mean values + SD. No significant differences were found (*t*-test).

4. RESULTS

As estimated by area measurement, the size of individual subfield layers in CA1 (Fig. 13), CA3 (Fig. 14) and the DG (Fig. 15) were similar in the two genotypes with the exception of the principal cell layer and stratum radiatum in CA3 which were significantly smaller (-13% and -16%, respectively) in Chst14 $-/-$ animals compared with Chst14 $+/+$ animals (Fig. 14).

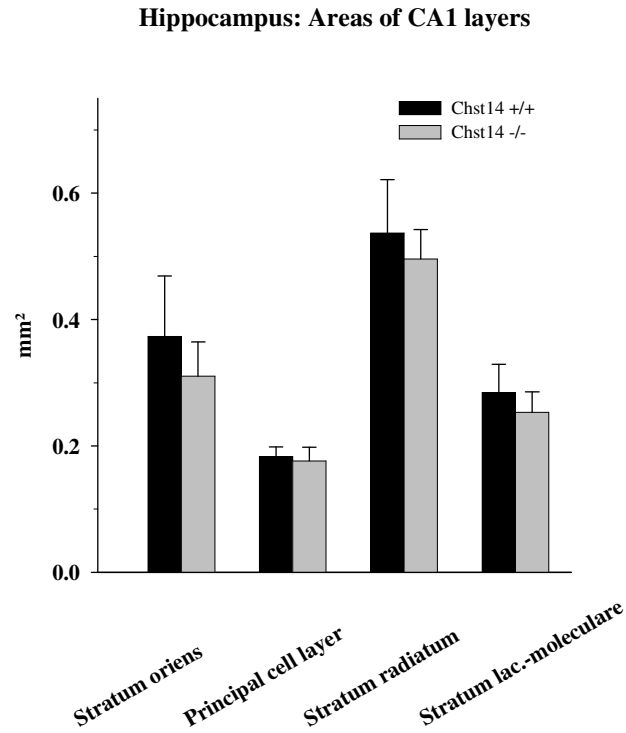


Figure 13: Areas of CA1 layers in coronal brain sections from Chst14 $+/+$ (black bars) and Chst14 $-/-$ animals (grey bars). Shown are averaged bilateral mean values + SD. No significant differences were found (t -test).

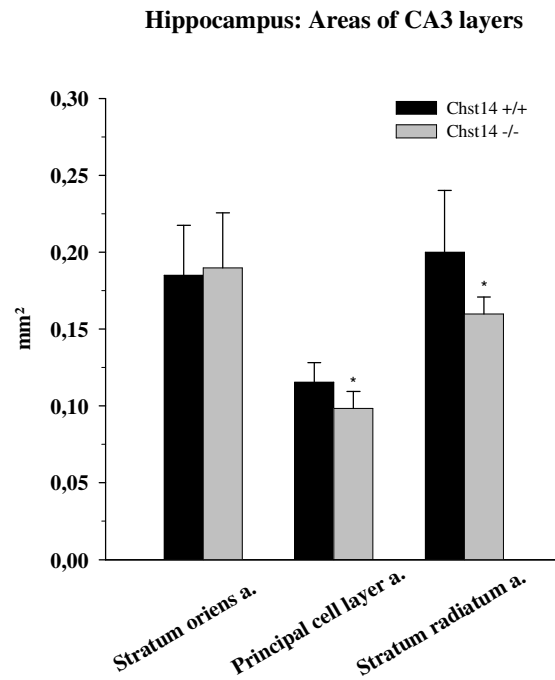


Figure 14: Areas of CA3 layers in coronal brain sections from Chst14 +/+ (black bars) and Chst14 -/- animals (grey bars). Shown are averaged bilateral mean values + SD. Asterisks indicate significant differences between the groups (*t*-test).

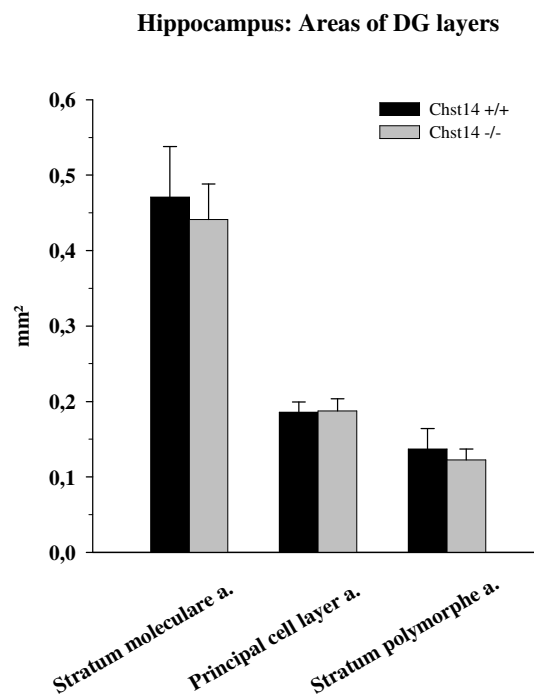


Figure 15: Areas of DG in coronal brain sections from Chst14 +/+ (black bars) and Chst14 -/- animals (grey bars). Shown are averaged bilateral mean values + SD. No significant differences were found (*t*-test).

4.2. Immunohistochemical markers, quality of staining and qualitative observations in Chst14 +/+ and Chst14 -/- animals

For each particular antigen, all sections were stained in the same primary and secondary antibody solutions kept in staining jars and stabilized in order to enable repeated long-term usage (Sofroniew and Schrell 1984; Irintchev et al. 2005). In this study, the previously documented reproducibility of this staining technique was also apparent: for all batches, the quality of staining remained constant in sections processed over a period of several months. No qualitative differences were noticed between Chst14 +/+ and Chst14 -/- animals in the staining patterns for the detected antigens. Fig. 16 shows examples of the stainings.

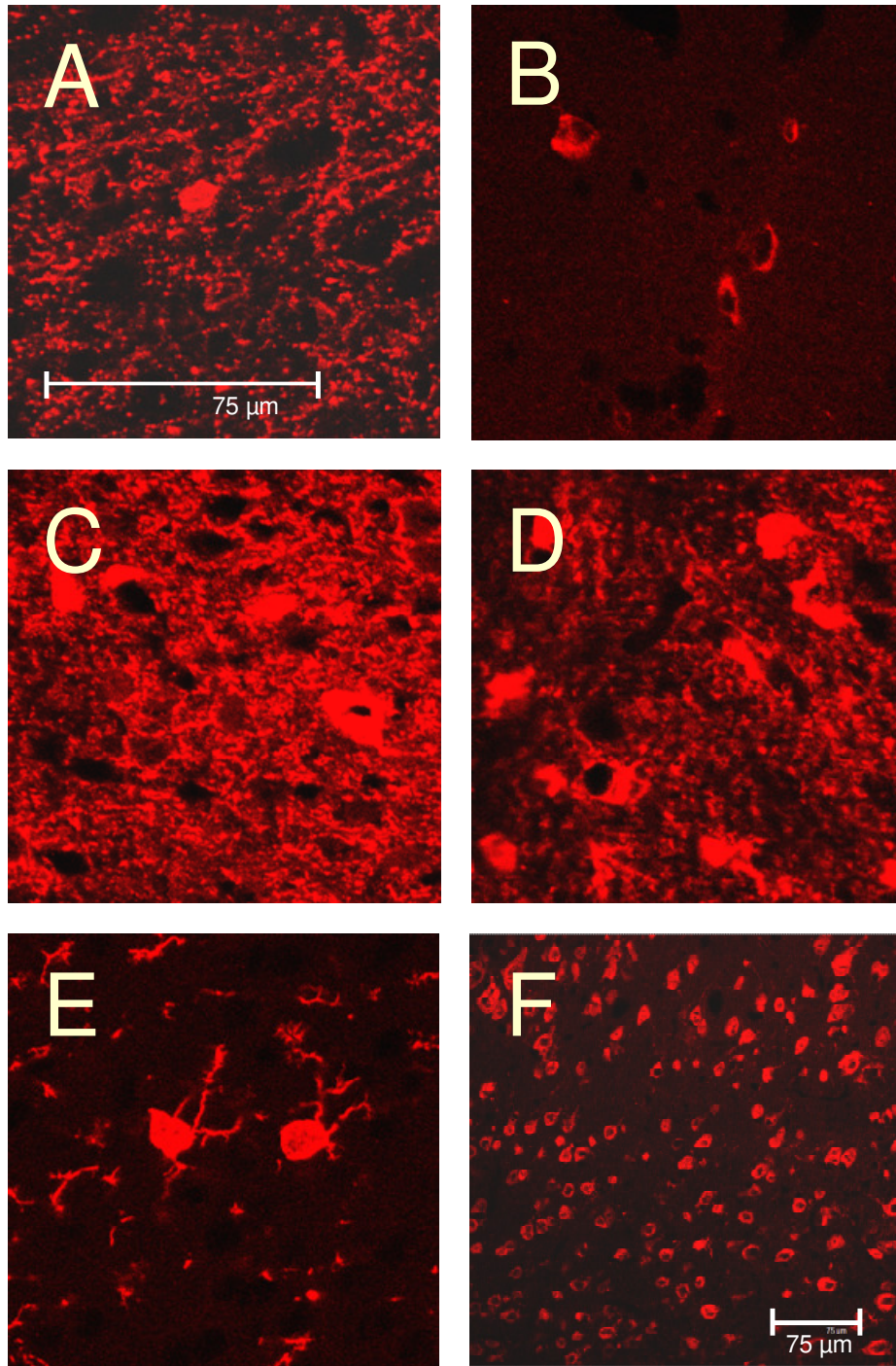


Figure 16: Examples of immunohistochemical stainings in the motor cortex of *Chst14*^{-/-} animals. A: CNPase; B: Reelin; C: PV; D: S-100; E: Iba1; F: NeuN. Scale bar in A indicates 75 μm for A-E. Scale bar in F indicates 75μm.

4.3. Stereological analysis of the motor cortex

4.3.1. General observations

Observation of nuclear stainings revealed an apparently normal structure of the motor cortex with the typical arrangement of cells in six layers. Furthermore, the distribution patterns of immunocytochemically identified cells were similar in Chst14 $-/-$ and Chst14 $+/+$ animals.

4.3.2. Total cell density

The numerical density (i.e. number per unit volume) of all cells, as a reference value indicative of global alterations in the motor cortex, was estimated by nuclear staining. The results showed no differences between Chst14 $-/-$ and Chst14 $+/+$ animals. Since the cortical thickness was similar in wild-type and mutant animals (Fig. 17), cell densities of all cells, as well as of all other cell types described below, reflect total number of cells in a cortical column (cell number under unit of cortical surface).

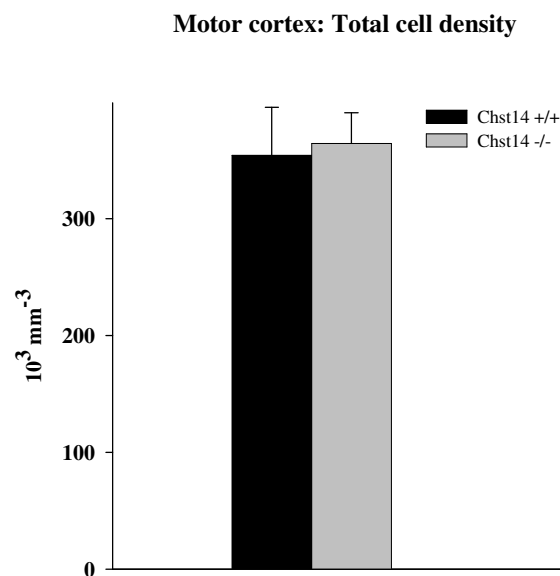


Figure 17: Numerical density of the total cell population, identified by nuclear staining in the motor cortex, of Chst14 $+/+$ (black bar) and Chst14 $-/-$ animals (grey bar). Shown are mean values + SD. No significant difference was found (t -test).

4. RESULTS

4.3.3. Total neuronal population

The density of all neurons (NeuN⁺) in the motor cortex of Chst14 ^{+/+} and Chst14 ^{-/-} mice was similar (Fig. 18).

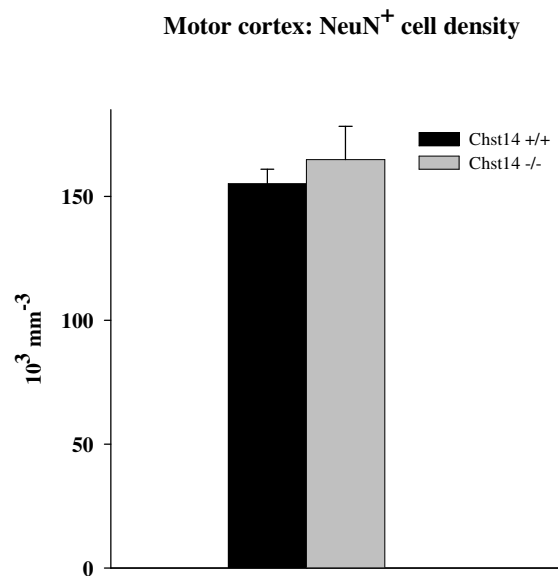


Figure 18: Numerical density of the total neuronal population in the motor cortex of Chst14 ^{+/+} (black bar) and Chst14 ^{-/-} animals (grey bar). Shown are mean values + SD. No significant difference was found (*t*-test).

4.3.4. Interneurons

Parvalbumin-positive and reelin-positive interneurons

The results of the density of PV⁺ and the reelin⁺ cells showed no significant differences in mutant animals compared to wild-type control animals (Fig. 19-20).

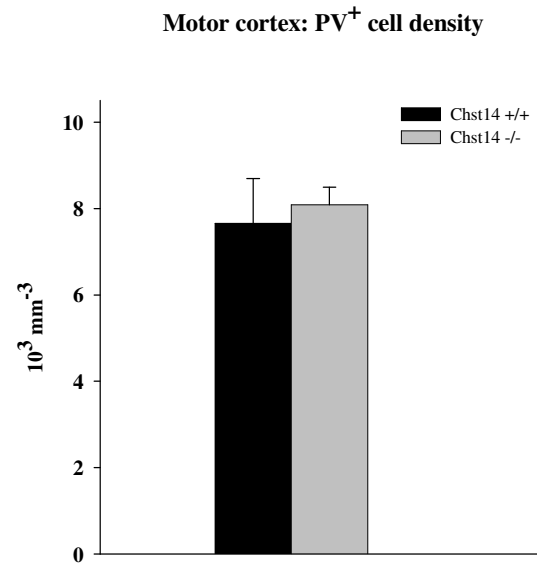


Figure 19: Numerical density of PV⁺ interneurons in the motor cortex of Chst14 +/+ (black bar) and Chst14 -/- animals (grey bar). Shown are mean values + SD. No significant difference was found (*t*-test).

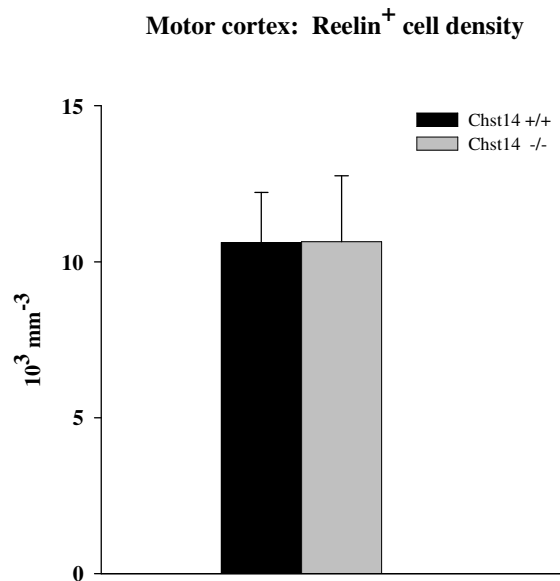


Figure 20: Numerical density of reelin⁺ interneurons in the motor cortex of Chst14 +/+ (black bar) and Chst14 -/- animals (grey bar). Shown are mean values + SD. No significant difference was found (*t*-test).

4. RESULTS

4.3.5. Glial cells

Astrocytes and oligodendrocytes

The estimation of numerical densities of S-100⁺ astrocytes (Fig. 21) and CNPase⁺ oligodendrocytes (Fig. 22) revealed no significant differences between Chst14 ^{-/-} and Chst14 ^{+/+} mice.

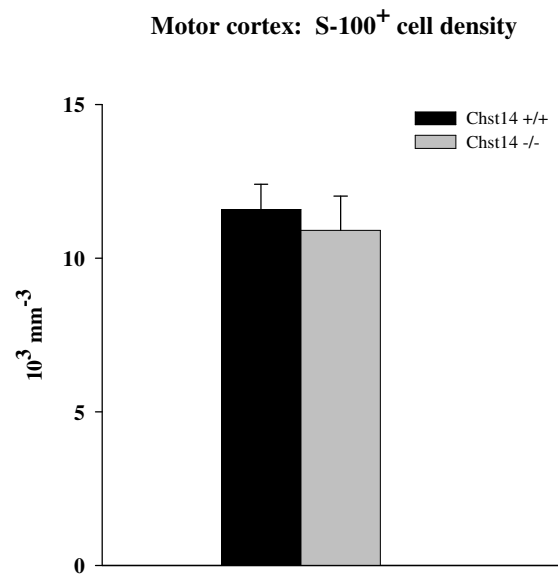


Figure 21: Numerical density of S-100⁺ astrocytes in the motor cortex of Chst14 ^{+/+} (black bar) and Chst14 ^{-/-} animals (grey bar). Shown are mean values + SD. No significant difference was found (*t*-test).

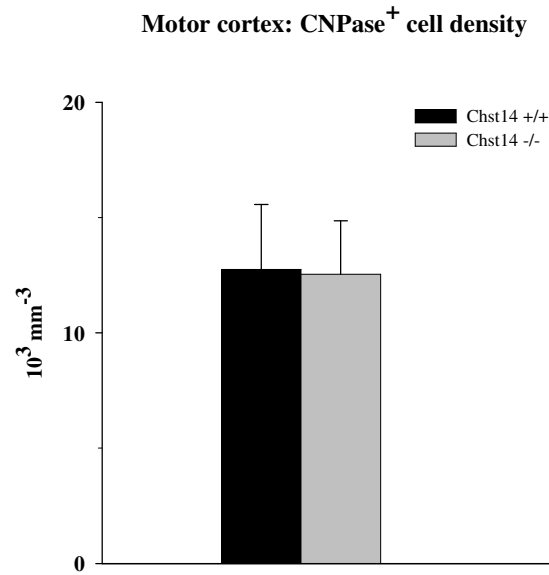


Figure 22: Numerical density of CNPase⁺ oligodendrocytes in the motor cortex of Chst14 +/+ (black bar) and Chst14 -/- animals (grey bar). Shown are mean values + SD. No significant difference was found (*t*-test).

4.3.6. Microglia

Iba1 is a recently discovered protein, involved in the activation of microglia and thus expressed in both quiescent and activated cells (Imai and Kohsaka, 2002). Reliable identification of both resting and activated microglial cells is possible as following activation the protein expression is enhanced and maintained at high level in active cells. Quantitative analysis of Iba1⁺ cells revealed a largely increased (+26%) number of microglial cells in Chst14 -/- animals as compared with wild-type animals (Fig. 23).

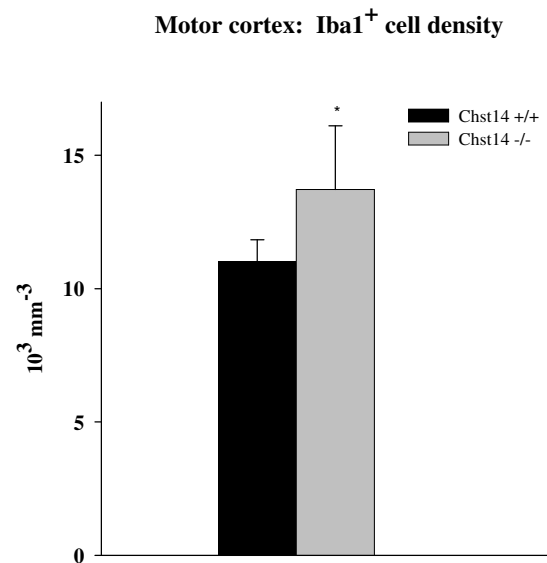


Figure 23: Numerical density of Iba1⁺ microglial cells in the motor cortex of Chst14 +/+ (black bar) and Chst14 -/- animals (grey bar). Shown are mean values + SD. Asterisk indicates a significant difference between the groups (*t*-test).

4.4. Stereological analysis of the hippocampus

4.4.1. Principal cell density

While density of the principal cells in the DG and the CA1 subfield showed no significant differences between the genotypes, in the CA3 subfield of Chst14 -/- mice a 24% decrease in the density of principal cells could be observed (Fig. 24).

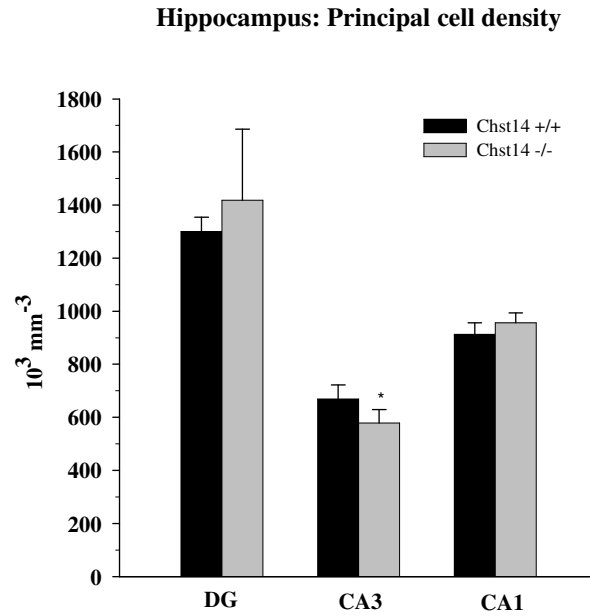


Figure 24: Principal cell density of the hippocampus of Chst14 +/+ (black bars) and Chst14 -/- animals (grey bars). Shown are mean values + SD. The asterisk indicates a significant difference between the groups (*t*-test).

4.4.2. Interneurons

Parvalbumin-positive and reelin-positive interneurons

A large (+26%), and statistically significant difference was found in the numerical density of parvalbumin-positive (PV⁺) interneurons in mutant animals compared with wild-type control animals in the CA3 subfield, whereas the densities in the DG and CA1 subfields were similar in both genotypes (Fig. 25). The results for reelin⁺ interneurons showed no difference in Chst14 -/- mice and Chst14 +/+ littermates (Fig. 26).

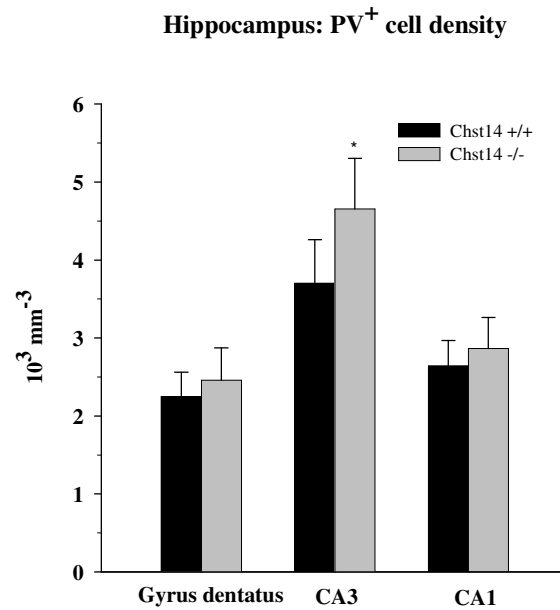


Figure 25: Numerical density of PV⁺ interneurons in the hippocampus of Chst14 +/+ (black bars) and Chst14 -/- animals (grey bars). Shown are mean values + SD. The asterisk indicates a significant difference between the groups (*t*-test).

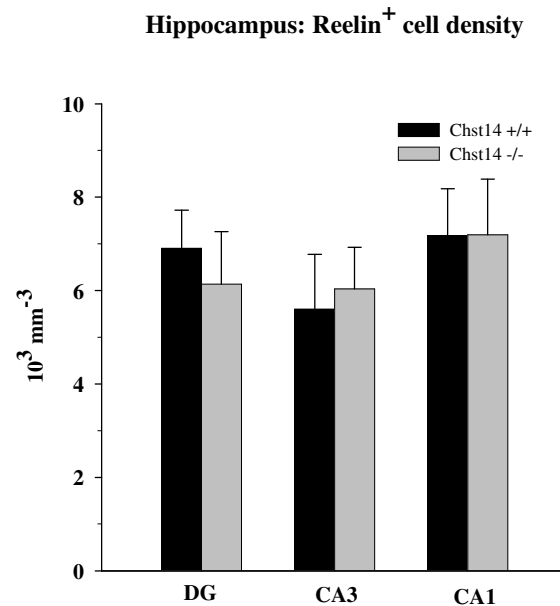


Figure 26: Numerical density of reelin⁺ interneurons in the hippocampus of Chst14 +/+ (black bars) and Chst14 -/- animals (grey bars). Shown are mean values + SD. No significant differences were found (*t*-test).

4. RESULTS

Estimation of numerical densities of different cell types in a reference volume allows calculation of physiologically meaningful ratios between cell types (Irintchev et al. 2005). Here we were interested whether the ratio of PV⁺ interneurons to principal cells, a parameter with relevance to the function of hippocampal subfields (Nikonenko et al. 2006). Since these two cell types are distributed in two different compartments within each subfield, PV⁺ cells in all layers of a subfield and principal cells only in the principal layer, we first calculated total numbers of each cell type per hippocampal subfield by multiplying numerical densities by reference volumes. The results obtained for total numbers of PV⁺ and principal cells were similar to those for numerical densities of these cell types in the three hippocampal subfields (data not shown). From total numbers per subfield, we then calculated the ratio of PV⁺ cells to principle cells and found a large (+76%) and significant increase in the CA3 subfield in Chst14 ^{-/-} compared with Chst14 ^{+/+} mice (Fig. 27). The ratios in the DG and CA1 were similar between the two genotypes (Fig. 27).

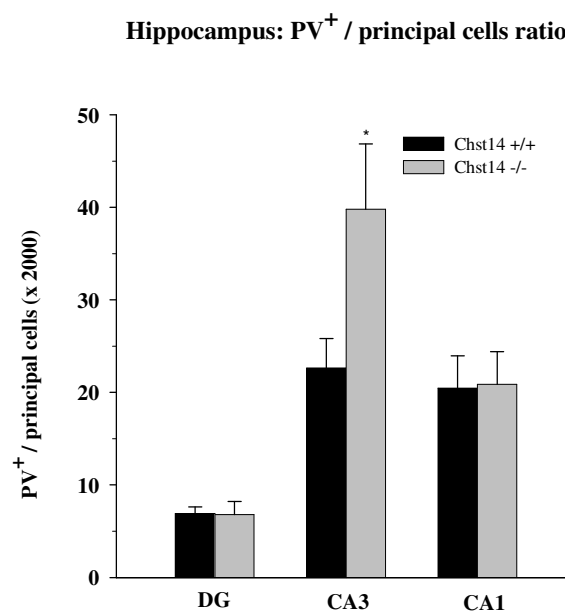


Figure 27: Ratio of PV⁺ cells to principal cells in the hippocampus of Chst14 ^{+/+} (black bars) and Chst14 ^{-/-} animals (grey bars). Shown are mean values + SD. The asterisk indicates a significant difference between the groups (*t*-test).

4.4.3. Glial cells

Microglia

In all subfields of the hippocampus, a large increase (+22% in the DG, +34% in CA3 and +36% in CA1) of Iba1⁺ cells in mutant mice compared with wild-type control animals was observed (Fig. 28). These findings are similar to those in the motor cortex (see 4.3.6).

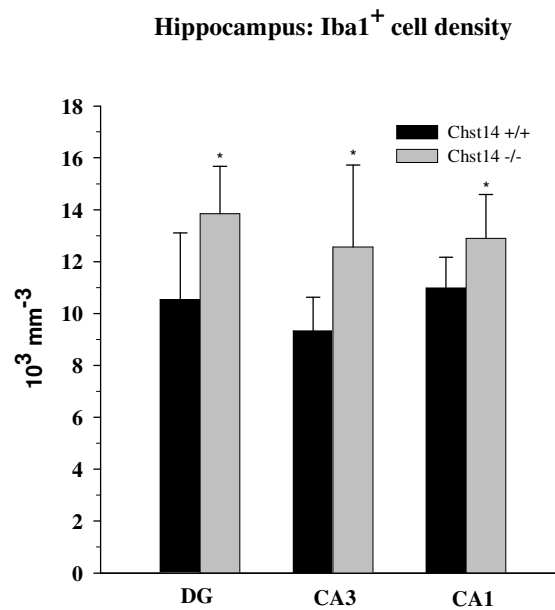


Figure 28: Cell density of Iba1⁺ microglial cells in the hippocampus of Chst14 +/+ (black bars) and Chst14 -/- animals (grey bars). Shown are mean values + SD. Asterisks indicate significant differences between the groups (*t*-test).

4.5. Analyses of soma size and synaptic coverage of principal neurons in CA1 and CA3 hippocampal subfields

4.5.1. Synaptic coverage

Since both number of PV⁺ interneurons and PV⁺/principal cell ratio are increased in Chst14 ^{-/-} mice compared with wild-type littermates, we wanted to see if the inhibitory input to pyramidal cells is also altered. Digitized confocal images were analyzed (see 3.5.4.) and densities of PV⁺ and PV⁻ GABAergic terminals, visualized by VGAT staining, on pyramidal cell bodies in the area CA1 and CA3 of hippocampus were estimated. Whereas in CA1 subfield of hippocampus the number of both PV⁺ and PV⁻ GABAergic terminals around pyramidal cell bodies was similar in Chst14 ^{-/-} mice compared with wild-type littermates, in CA3 subfield of Chst14 ^{-/-} mice these numbers were significantly reduced (-13% respectively; Fig. 29-30).

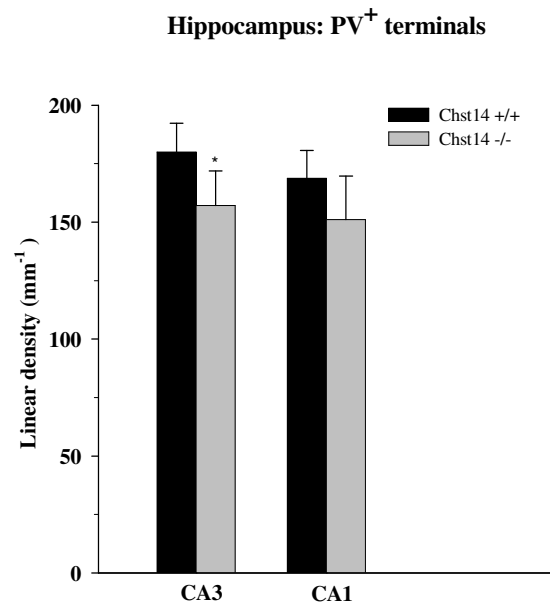


Figure 29: Densities of PV⁺ terminals on principal cells in the CA3 and CA1 subfields of the hippocampus of Chst14 +/+ (black bars) and Chst14 -/- animals (grey bars). Shown are mean values + SD. The asterisk indicates a significant difference between the groups (*t*-test).

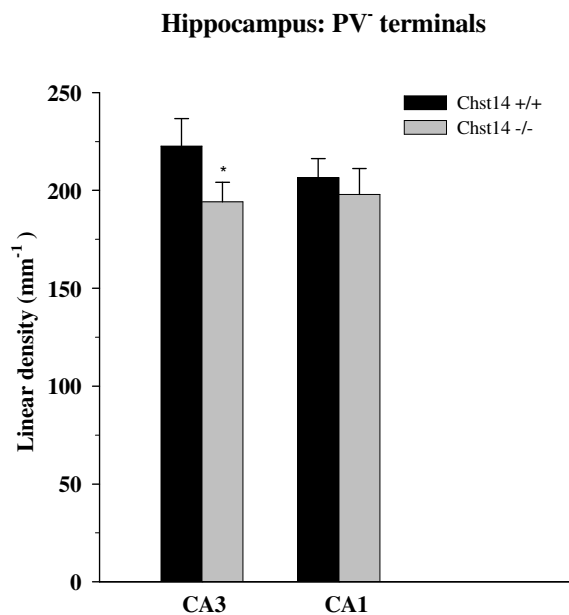


Figure 30: Densities of PV⁻ terminals on principal cells in the CA3 and CA1 subfields of the hippocampus of Chst14 +/+ (black bars) and Chst14 -/- animals (grey bars). Shown are mean values + SD. The asterisk indicates a significant difference between the groups (*t*-test).

4. RESULTS

During analysis of the digitized confocal images (see 3.5.4.), the size of pyramidal cell bodies in the area CA1 and CA3 was also estimated and statistical comparisons revealed no significant difference between the genotypes (Fig. 31).

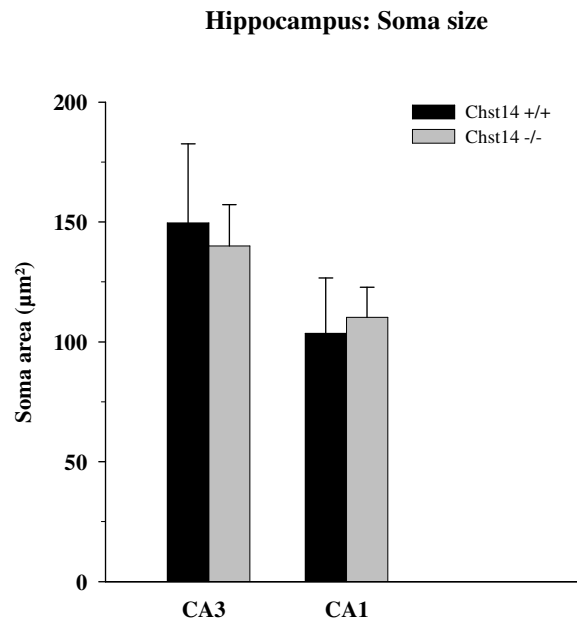


Figure 31: Soma size of pyramidal cells in the CA3 and CA1 subfields of the hippocampus of Chst14 +/+ (black bars) and Chst14 -/- animals (grey bars). Shown are mean values + SD. No significant differences were found (*t*-test).

5. DISCUSSION

The results of this study provide novel evidence for the functional importance of Chst14 for development of the motor cortex and the hippocampus. Studying Chst14 ^{-/-} and wild-type control mice, we observed that constitutive deletion of Chst14 in the mouse causes a range of abnormalities in the hippocampus and motor cortex. The results summarized in Table 3 show genotype-specific changes in gross-anatomical parameters, neuronal and glial subpopulations and in synaptic coverage.

Gross-anatomical parameters

Body weight	↓ -21%
Brain mass	=

Motor cortex

Cortical thickness	=
Total cell density	=
Total neuronal density	=
PV ⁺ cell density	=
Reelin ⁺ cell density	=
S-100 ⁺ cell (astrocyte) density	=
CNPase ⁺ cell (oligodendrocyte) density	=
Iba1 ⁺ cell (microglia) density	↑ +26%

5. DISCUSSION

Dorsal hippocampus

	DG	CA3	CA1
Total subfield volume	=	=	=
Principal cell layer volume	=	↓ -13%	=
Stratum radiatum volume		↓ -16%	=
Stratum oriens volume		=	=
Str. lac.-molecularare volume			=
Str. molec. & polym. volume	=		
Principal cell density	=	↓ -24%	=
PV ⁺ cell density	=	↑ + 26%	=
PV ⁺ cell number	=	↑ +28%	=
PV ⁺ /principal cells ratio	=	↑ +76%	=
Reelin ⁺ cell density	=	=	=
Iba1 ⁺ cell (microglia) density	↑ +22%	↑ +34%	↑ +36%
Soma size of pyramidal neurons		=	=
PV ⁺ perisomatic terminals		↓ -13%	=
PV ⁻ perisomatic terminals		↓ -13%	=

Table 3: Summary of morphological results for Chst14 ^{+/+} and Chst14 ^{-/-} littermates studied at 2 months of age. Arrows indicate lower (↓) or higher (↑) values in the knockout mice as compared to the control animals, = indicates no significant difference.

5.1. Morphological aberrations in Chst14 ^{-/-} mouse

5.1.1. Gross morphological variables

Analysis of the 2-month-old mice revealed that the body weight in the Chst14 ^{-/-} mice was decreased by 21% compared with gender-matched wild-type littermates. The decrease of the body weight can be explained by decreased weights of bones (tibia) and organs like heart, liver, and kidney. Interestingly, the decrease of body weight in Chst14 ^{-/-} mice is dependent on the genetic background, becoming more severe with further backcrossing to C57BL6/J background (Nuray Akyüz, personal communication). This is not unusual, since the C57BL/6J background seems to confer a susceptibility to genetic insults. For example, neural cell adhesion molecule L1-deficient mice on a C57BL6/J background are smaller than the wild-type littermates and have numerous CNS abnormalities, whereas on 129SV/J background the mutants have normal body size and their brains are more subtly affected than knockout mice on C57BL6/J background (Dahme et al. 1997; Guseva et al. 2009). Regarding the Chst14 deficiency, two findings can explain the decrease in body weight. First, there is high expression of DS in the proteoglycans byglycan and decorin, present in bone and cartilage, and double knockout mice for these two molecules are also small in size (Corsi et al. 2002). Second, Chst14 is expressed in the pituitary gland at a higher level than in other brain regions and Chst14 deficiency causes a significant downregulation of the thyroid stimulating hormone levels during the postnatal development (Nuray Akyüz, personal communication). In contrast to body weight, brain weight, hippocampal size and cortical thickness in Chst14 ^{-/-} mice are similar to these in the wild-type littermates indicating that brain development in Chst14 ^{-/-} mice is less severely affected compared with other organs. Moderate deficits in Chst14 ^{-/-} mice were only detectable in the CA3 area of the hippocampus: The volume of the principal cell layer and stratum radiatum were 13% and 16% smaller, respectively, in Chst14 ^{-/-} versus Chst14 ^{+/+} animals (Table 3 and Fig. 14). These volume reductions are entirely explainable by loss of pyramidal neurons in the CA3 region (see also 5.1.2.). Decreased size of the pyramidal cell layer and decreased pyramidal cell density indicate that the total number of pyramidal neurons in CA3 is lower in Chst14 ^{-/-} mice than in their Chst14 ^{+/+} littermates. Decreased number of pyramidal neurons can also cause reduction in the volume of stratum radiatum since the pyramidal apical dendrites reside in this layer.

5.1.2. Cell populations affected by the mutation in the Chst14 gene

The Iba1⁺ microglial cells were more numerous in Chst14 ^{-/-} than in Chst14 ^{+/+} mice in all studied areas, motor cortex (+26%), hippocampal subfields CA1 (+36%), CA3 (+34%) and the DG (+22%; Table 3, Fig. 23 and 28). Microgliosis is primarily associated with brain tissue damage as a result of, for example, trauma, degenerative, inflammatory, or autoimmune diseases. We could not see apparent signs of microglial cell activation, for example increase in cell body size and reduced ramification (Streit et al. 1999), or neuronal cell death in the areas analyzed in Chst14 ^{-/-} mice. Astrogliosis, a typical sign of brain damage, was also not observed in the studied brain regions. Still, the present observations cannot exclude the possibility of a slowly progressing degenerative process in 2-month-old Chst14 ^{-/-} mice. A definite answer of question of neuronal degeneration can be provided by future analyses of neuronal cell numbers in older mice. Yet another explanation of the observed microgliosis is enhanced synaptic elimination. Microglial numbers are, for example, drastically enhanced in the absence of neuronal degeneration during the process of “synaptic stripping”, i.e. deafferentation after motoneuron axotomy (Moran and Graeber 2004). Here I found reduced numbers of PV/VGAT⁺ synaptic terminals in the CA3 subfield of Chst14 ^{-/-} mice. By itself, this observation cannot explain the general increase in microglia density in all studied regions, but gives support of the notion that microgliosis in Chst14^{-/-} mice could be related to abnormal synaptic structure and/or function. This notion is conceivable because CS/DS are important for the organization of the extracellular matrix the CNS and this matrix is of crucial importance for synaptic targeting, stabilization, and function (Dityatev and Schachner 2003; Dityatev et al. 2010)

Next we analyzed densities of excitatory neurons (pyramidal and granular cells) in the three hippocampal areas using nuclear staining to identify the cells. The numerical density (number per unit volume) of principal cells were similar in DG and CA1 of Chst14 ^{-/-} and Chst14 ^{+/+} mice, whereas it was decreased in the CA3 subfield of the hippocampus of Chst14 ^{-/-} (24%). It is difficult to explain the reduction in number of CA3 pyramidal cells in Chst14 ^{-/-} mice. Cell loss could be related to a region-specific enhancement of cell death during early development of the hippocampus but currently no mechanism for such enhancement can be envisaged. Alternatively, it can be speculated that abnormal targeting of synaptic connections to CA3 pyramidal neurons in the mutants leads to neuronal death during postnatal establishment and maturation of synaptic circuitries. Such an explanation has been proposed

5. DISCUSSION

for neural cell adhesion molecule (NCAM)-deficient mice in which, similar to *Chst14*^{-/-} mice, the number of principal neurons is reduced in CA3 but not in CA1 or the DG (Andrey Irintchev, personal communication). The idea of deficient wiring and synaptic dysfunction in the *Chst14*^{-/-} mouse is compatible with the finding of neuronal loss in CA3 and microgliosis in all brain areas analyzed.

PV⁺ interneurons are the main subpopulation of GABAergic interneurons in the hippocampus and DS-carrying proteoglycans are accumulated in perineuronal nets surrounding these cells (Dityatev and Schachner 2003). My results revealed a significant increase in density of PV⁺ interneurons in the CA3 subfield of the hippocampus of *Chst14*^{-/-} mice compared to *Chst14*^{+/+} littermates, while no other subfield of the hippocampus was affected. Additionally, the population of reelin⁺ interneurons, which comprise the majority of PV⁺ hippocampal interneurons (Pesold et al. 1999), was also not altered in *Chst14*^{-/-} mice. Currently, it is not possible to explain the CA3 region-specific increase in PV⁺ cell in the *Chst14*^{-/-} mice. Deficits in perineuronal nets is an unlikely cause as these nets surround PV⁺ interneurons in all hippocampal subfields. A reasonable speculation is that abnormal numbers of PV⁺ neurons in the mutant mouse result from aberrant connectivity, similar to the deficit in CA3 pyramidal neurons. More important is the consideration that the abnormality in PV⁺ interneurons could have significant, yet unidentified functional consequences (5.1.3.). Interneurons play a crucial role in modulating and synchronizing cortical output of the pyramidal cells. They are thought to affect the postnatal development of cortical circuitry by feed-forward and feedback inhibition of active pyramidal neurons. Hundreds of principal neurons are innervated by single inhibitory neurons (Halasy et al. 1996). Hence PV⁺ interneurons are well suited to synchronize cortical network activity (Galarreta et al. 1999; Gibson et al. 1999) in different frequency bands (Cobb et al. 1995; Ylinen et al. 1995; Tamas et al. 2000; Szabadics et al. 2001). The major proportion of GABAergic cells in the hippocampus and cerebral cortex consist of PV⁺ interneurons (Fukuda and Kosaka 2000; Galarreta and Hestrin 2002). In the hippocampus, the majority of PV⁺ interneurons belong to the group of perisomatic inhibitory neurons (Kosaka et al. 1987; Freund and Buzsaki 1996; Maccaferri et al. 2000). Electrophysiologically, they have been characterized as fast-firing cells (Kawaguchi et al. 1987). These inhibitory neurons are coupled by both chemical and electrical synapses and form an inhibitory network, which operates at high-frequency discharge rates. This network has a strong impact on neuronal excitability and, thus, regulates basic physiological properties such as synchronization and oscillatory activities in the

hippocampus and in the cortex. Therefore, changes in the PV⁺ interneuron-mediated inhibition have profound effects on hippocampal and cortical function. In order to understand comprehensively the aberrations in the mutant animals, we also analyzed the relative proportions of PV⁺ interneurons and the principal cells. The ratio of PV⁺ interneurons to principal cells was highly increased (76%) in the CA3 subfield of Chst14 ^{-/-} mice compared with Chst14 ^{+/+} littermates indicating that a higher-than-normal number of inhibitory interneurons innervate a single principal neuron. This finding prompted the analysis of the GABAergic synaptic coverage on the pyramidal neurons.

5.1.3. Synaptic coverage of pyramidal neurons in the hippocampus

The analysis of the synaptic coverage of pyramidal cells in the CA1 and CA3 regions of the hippocampus revealed a decreased linear density of both PV⁺ and PV⁻ synapses on cell bodies of pyramidal cells in the CA3 region of Chst14 ^{-/-} mice, whereas in the CA1 region there was no significant difference between the genotypes. The decrease in PV⁺ synapses was somewhat unexpected considering the increased PV⁺ interneuron to principal cell ratio in the CA3 of Chst14 ^{-/-} mice. Analyses of mice deficient in the adhesion molecules CHL1 and tenascin R, for example, also revealed increased densities of PV⁺ interneurons, and increased interneuron/principal cell ratios in the hippocampus, but, in both cases they were accompanied by the finding of increased perisomatic inhibition (Nikonenko et al. 2006; Morellini et al. 2010). The finding of the reduced perisomatic inhibition in Chst14 ^{-/-} mice represents the first evidence for the role of dermatan sulfate epitopes in synapse formation/maintenance. Importantly, the abnormality affects both PV⁺ and PV⁻ terminals, which originate from two different types of basket cell, PV⁺ cholecystokinin-negative (CCK⁻) and PV⁻ CCK⁺ interneurons (Maccaferri et al. 2000; Somogyi and Klausberger 2005). These deficits might be functionally important and warrant further behavioral and electrophysiological studies (see 5.2.).

5.1.4. Cell populations unaffected by the mutation in the Chst14 gene

Our study revealed no differences between Chst14 ^{-/-} and Chst14 ^{+/+} mice with regard to numerical densities of neuronal populations in the motor cortex and in the hippocampal subfields CA1 and DG. The numerical densities of astrocytes and oligodendrocytes in all studied regions were also similar between the genotypes. This could be interpreted as a hint

that dermatan sulfates are dispensable for the formation and maintenance of these major cellular populations. A conclusion like this appears, however, superficial. In this study, we have evaluated a single variable with regard to these cellular populations, namely, the cell number. Other aspects such as functional cell properties, neuronal connectivity, dendritic tree morphologies and dendritic spine densities, which might be substantially altered as a result of the gene mutation, were not analyzed in this study.

5.2. Possible functional significance of the structural aberrations in Chst14 deficient mice

The abnormally high number of microglial cells in Chst14 ^{-/-} animals was surprising with regard to the normal number of astrocytes, normal numerical densities of most neuronal populations, and lack of apparent signs of an inflammatory or a degenerative response in Chst14 ^{-/-} mice. It is tempting to speculate that the involvement of dermatan sulfates in synaptic formation, maintenance and/or function causes synaptic abnormalities in Chst14 ^{-/-} mice, which in turn results in increased microglial cell densities in the still developing young adult mice. Microglial cells produce cytokines, neurotransmitters, neuromodulators, and neurotrophins, for example glutamate, nitric oxide and brain-derived neurotrophic factor, that can influence synaptic function (Bessis et al. 2007). Thus, abnormal numbers of microglial cells can further enhance existing or cause additional behavioral and physiological aberrations.

Considering that all studied brain regions of Chst14 ^{-/-} mice were equally affected by microgliosis, it can also be proposed that the effect of the mutation on microglia is autonomous. This notion is supported by well documented involvement of DS in immune response, for example, by stimulation of macrophage nitric oxide production (Wrenshall et al. 1999; Leteux et al. 2000). Interestingly, treatment of rats with experimental autoimmune encephalomyelitis with DS suppresses the disease progression (Inaba et al. 1999). It is possible that dermatan sulfates play a role in homeostasis of microglial cells in the brain. If this hypothesis is true, the responses of the Chst14 ^{-/-} mice to injury of the nervous system should be altered, a notion which warrants further investigations.

The search of functional and behavioral abnormalities in Chst14 ^{-/-} mice is still in progress. Currently existing data show that although Chst14 ^{-/-} mice walk normally, their performance

5. DISCUSSION

is poor in motor tests that are more challenging than overground locomotion, the rotarod and the pole test (Nuray Akyüz, personal communication; Nickel 2009). These deficits in the motor performance possibly have other origins than the motor cortex as this cortical area in Chst14 ^{-/-} mice appeared, as analyzed here, normal except for the microgliosis discussed above. Impaired motor coordination cannot also be explained by hippocampal deficits as the hippocampus is barely involved in coordination of movements.

The hippocampus belongs to the limbic system and is essential mediating memory formation, novelty detection and spatial navigation in rodents (Leuner and Gould 2010). The hippocampus consists of a heterogeneous population of neurons distinguished by their morphological characteristics, and connectivity. The synapses and dendrites of mature neurons undergo continuous rearrangement, and entirely new neurons are formed throughout life. These various forms of structural change, which are typically associated with development, continue to occur during the postnatal period and beyond, persisting into young adulthood and throughout middle age and senescence. Our study of 2-month-old, thus young adult mice, gives the first insight into functions of dermatan sulfates in hippocampal development and early plasticity. Since the hippocampus is a brain structure that displays high level of plasticity throughout life, it is warranted to study Chst14 ^{-/-} mice also at later time-points. The morphological analysis of 2-month-old Chst14 deficient mice revealed that the CA3 subfield of the hippocampus is specifically affected including reduction of principal cell number, increased number of PV⁺ cells and ratio PV⁺/principal cells and reduced perisomatic inhibitory input to pyramidal cell bodies. These region-specific affects could be explained if DS carrying molecules are highly concentrated in the CA3 subfield as opposed to other hippocampal areas. To the best of my knowledge, no evidence of such a region-specific accumulation exists. Therefore, currently it can be speculated that structural deficits in the CA3 region of the Chst14 ^{-/-} mouse have their origins in aberrant connectivity. Considering the findings of this study and the specific involvement of CA3 in working memory and novelty detection (Kesner 2007), it would be very interesting to investigate these behavioral traits in Chst14 ^{-/-} mice.

5.3. Conclusion

The present study has identified structural aberrations in the Chst14 - deficient mouse, which indicate possible involvement of this enzyme in the control of microglial numbers in the central nervous system, as well as a very specific role in the development of the hippocampus. Altered densities of synapses and interneurons in the CA3 region of the hippocampus suggest a specific role of Chst14 in learning and memory, but further experiments are needed to confirm this hypothesis. Our results indicate that detailed electrophysiological and behavioral investigation of Chst14 ^{-/-} mice would be interesting, and indeed needed, to understand the functional impact of the structural changes described here. An interesting finding of increased microglial densities in all CNS regions studied in the absence of evidence for microglial activation or inflammation or abnormal cell death in Chst14 ^{-/-} mice suggests an involvement of Chst14 in the homeostatic negative regulation of microglial numbers. Alternatively, microgliosis in Chst14 ^{-/-} mice might reflect abnormal synaptic turnover as a consequence of abnormal development of connectivity in functional ensembles. This first morphological study of the Chst14 ^{-/-} mouse indicate that this mutant is a promising model, which could contribute to further understanding of the roles of dermatan sulfates under normal and pathological conditions.

6. SUMMARY

Chondroitin/dermatan sulfate proteoglycans are major components of the extracellular matrix important for cell migration and axonal pathfinding. The different chondroitin/dermatan sulfate structures are generated by sulfation and epimerisation of glucuronic/iduronic acid. In order to distinguish between functions of chondroitin and dermatan sulfates, a mouse deficient in dermatan-4O-sulfotransferase1 (Chst14 $-/-$), the key enzyme indispensable for the formation of iduronic acid-containing blocks in dermatan sulfates, has been recently created. In order to uncover the roles of dermatan sulfates in cortical development, I studied these Chst14 $-/-$ mice with respect to morphological abnormalities in the motor cortex and hippocampus, well-defined brain structures known to be functionally relevant for higher brain functions including learning and memory. Morphometric as well as stereological analyses of immunohistochemically identified major cell types (neurons, neuronal subpopulations, astrocytes, oligodendrocytes and microglia) were performed on 2-month-old Chst14 $-/-$ mice and wild-type (Chst14 $+/+$) littermates. Analyses of gross anatomical variables revealed that Chst14 $-/-$ mice had significantly reduced body weight (-21%) compared with Chst14 $+/+$ littermates, which could be explained by reduction in the mass of bones, heart, liver, kidneys and other organs. In contrast, the Chst14 $-/-$ brains were normal in size and had no gross morphological abnormalities. The cortical thickness in the motor cortical area as well as the total area of the hippocampus and its subfields were also not altered in Chst14 $-/-$ mice. However, the pyramidal cell layer and stratum radiatum in CA3 were reduced in size by 13% and 16%, respectively, in Chst14 $-/-$ compared with Chst14 $+/+$ mice. Additionally, the numerical density of pyramidal cells was reduced by 24% and density of parvalbumin-positive (PV⁺) interneurons was increased by 26% in the CA3 region of Chst14 $-/-$ mice. Since PV⁺/principal cell ratio in the CA3 of Chst14 $-/-$ was by 76% higher than in Chst14 $+/+$ mice, I also analyzed densities of perisomatic inhibitory terminals on pyramidal cells using confocal microscopy. While in the CA1 region there was no difference between the genotypes, the terminal density was reduced by 13% in the CA3 of Chst14 $-/-$ compared with Chst14 $+/+$ mice. Other regions of the hippocampus as well as the motor cortex were not affected by the mutation. Major cell populations, including total cell numbers and NeuN⁺ neurons in the cortex, principal cells in the hippocampus, PV⁺ and reelin⁺ interneurons, CNPase⁺ oligodendrocytes and S100⁺ astrocytes had similar densities in the two genotypes. One notable exception was Iba1⁺ microglia, which was increased in density in all studied areas (motor cortex +26%; CA1 +36%; CA3 +34%; DG +22%). This study gives important

6. SUMMARY

first insights into the structural changes in the brain caused by Chst14 deletion. Further electrophysiological and behavioural experiments are needed to understand the functional consequences of the observed structural aberrations and the role of Chst14 and dermatan sulfates in neural development and plasticity.

7. REFERENCES

Abo T, Balch CM (1981) A differentiation antigen of human NK and K cells identified by a monoclonal antibody (HNK-1). *J Immunol* 127: 1024–1029.

Baenziger JU (2003) Glycoprotein hormone GalNAc-4-Sulphotransferase. *Biochem Soc Trans* 31: 326–330.

Bandtlow CE, Zimmermann DR (2000) Proteoglycans in the developing brain: new conceptual insights for old proteins. *Physiol Rev* 80: 1267–1290.

Bao X, Mikami T, Yamada S, Faissner A, Muramatsu T, Sugahara K (2005) Heparin-binding growth factor, pleiotrophin, mediates neuritogenic activity of embryonic pig brain-derived chondroitin sulfate/dermatan sulfate hybrid chains. *J Biol Chem* 280: 9180–9191.

Bao X, Nishimura S, Mikami T, Yamada S, Itoh N, Sugahara K (2004) Chondroitin sulfate/dermatan sulfate hybrid chains from embryonic pig brain, which contain a higher proportion of L-iduronic acid than those from adult pig brain, exhibit neuritogenic and growth factor binding activities. *J Biol Chem* 279: 9765–9776.

Beighton P, De Paepe A, Steinmann B, Tsipouras P, Wenstrup RJ (1998) Ehlers-Danlos syndromes: revised nosology, Villefranche, 1997. Ehlers-Danlos National Foundation (USA) and Ehlers-Danlos Support Group *Am J Med Genet* 77: 31–7.

Bessis A, Béchade C, Bernard D, Roumier A (2007) Microglial control of neuronal death and synaptic properties. *Glia* 55: 233–238.

Bernfield M, Sanderson RD (1990) Syndecan, a developmentally regulated cell surface proteoglycan that binds extracellular matrix and growth factors. *Phil Trans R Soc Lond Ser B* 327: 171–186.

Bovolenta P, Feraud-Espinosa I (2000) Nervous system proteoglycans as modulators of neurite outgrowth. *Prog Neurobiol* 61: 113–132.

Bowman KG, Bertozzi CR (1999) Carbohydrate sulfotransferases: mediators of extracellular communication. *Chem Biol* 6: R9–R22.

Chaudhry FA, Reimer RJ, Bellocchio EE, Danbolt NC, Osen KK, Edwards RH, Storm-Mathisen J (1998) The vesicular GABA transporter, VGAT, localizes to synaptic vesicles in sets of glycinergic as well as GABAergic neurons. *The Journal of Neuroscience* 18: 9733–9750.

Cheng F, Heinegard D, Malmstrom A, Schmidtchen A, Yoshida K, Fransson LA (1994) Patterns of uronosyl epimerization and 4-/6-O-sulphation in chondroitin/dermatan sulphate from decorin and biglycan of various bovine tissues. *Glycobiology* 4: 685–696.

7. REFERENCES

- Cobb SR, Buhl EH, Halasy K, Paulsen O, Somogyi P (1995) Synchronization of neuronal activity in hippocampus by individual GABAergic interneurons. *Nature* 378: 75–78.
- Corsi A, Xu T, Chen XD, Boyde A, Liang J, Mankani M, Sommer B, Iozzo RV, Eichstetter I, Robey PG, Bianco P, Young MF (2002) Phenotypic effects of biglycan deficiency are linked to collagen fibril abnormalities, are synergized by decorin deficiency, and mimic Ehlers-Danlos-like changes in bone and other connective tissues. *J Bone Miner Res* 17: 1180–1189.
- Dahme M, Bartsch U, Martini R, Anliker B, Schachner M, Mantei N (1997) Disruption of the mouse L1 gene leads to malformations of the nervous system. *Nat Genet* 17: 346–349.
- Dündar M, Demiryilmaz F, Demiryilmaz I, Kumandas S, Erkilic K, Kendirci M, Tuncel M, Ozyazgan I, Tolmie JL (1997) An autosomal recessive adducted thumb-club foot syndrome observed in Turkish cousins. *Clin Genet* 51: 61–64.
- Dündar M, Kurtoglu S, Elmas B, Demiryilmaz F, Candemir Z, Ozkul Y, Durak AC (2001). A case with adducted thumb and club foot syndrome. *Clin Dysmorphol* 10: 291–293.
- Dündar M, Müller T, Zhang Q, Pan J, Steinmann B, Vodopiutz J, Gruber R, Sonoda T, Krabichler B, Utermann G, Baenziger JU, Zhang L, Janecke AR (2009) Loss of dermatan-4-sulfotransferase 1 function results in adducted thumb-clubfoot syndrome. *Am J Hum Genet* 85: 873–82.
- Dityatev A, Schachner M (2003) Extracellular matrix molecules and synaptic plasticity. *Nat Rev Neurosci* 4: 456–68
- Dityatev A, Schachner M, Sonderegger P (2010) The dual role of the extracellular matrix in synaptic plasticity and homeostasis. *Nat Rev Neurosci* 11: 735–46.
- Evers MR, Xia G, Kang HG, Schachner M, Baenziger JU (2001) Molecular cloning and characterization of a dermatan-specific N-acetylgalactosamine, 4-O-sulfotransferase. *J Biol Chem* 276: 36344–36353.
- Fernandez JA, Petaja J, Griffin JH (1999) Dermatan sulfate and LMW heparin enhance the anticoagulant action of activated protein C. *Thromb Haemost* 82: 1462–1468.
- Fransson LA, Belting M, Jonsson M, Mani K, Moses J, Oldberg A (2000) Biosynthesis of decorin and glypican. *Matrix Biol* 19: 367–376.
- Freund TF, Buzsaki G (1996) Interneurons of the hippocampus. *Hippocampus* 6: 347–470.
- Fukuda M, Hiraoka N, Akama TO, Fukuda MN (2001) Carbohydrate-modifying sulfotransferases: structure, function, and pathophysiology. *J Biol Chem* 276: 47747–47750.

7. REFERENCES

- Fukuda T, Kosaka T (2000) Gap junctions linking the dendritic network of GABAergic interneurons in the hippocampus. *J Neurosci* 20: 1519–1528.
- Galarreta M, Hestrin S (1999) A network of fast-spiking cells in the neocortex connected by electrical synapses. *Nature* 402: 72–75.
- Garman RH (1990) Artifacts in routinely immersion fixed nervous tissue. *Toxicol Pathol* 18: 149–153.
- Gibson JR, Beierlein M, Connors B (1999) Two networks of electrically coupled inhibitory neurons in neocortex. *Nature* 402: 75–79.
- Guseva D, Angelov DN, Irintchev A, Schachner M (2009) Ablation of adhesion molecule L1 in mice favours Schwann cell proliferation and functional recovery after peripheral nerve injury. *Brain* 132: 2180–2195.
- Habuchi O (2000) Diversity and functions of glycosaminoglycan sulfotransferases. *Biochem. Biophys Acta* 1474: 115–127.
- Halasy K, Buhl EH, Lorinczi Z, Tamas G, Somogyi P (1996) Synaptic target selectivity and input of GABAergic basket and bistratified interneurons in the CA1 area of the rat hippocampus. *Hippocampus* 6: 306–329.
- Hikino M, Mikami T, Faissner A, Vilela-Silva AC, Pavao MS, Sugahara K (2003) Oversulfated dermatan sulfate exhibits neurite outgrowth-promoting activity toward embryonic mouse hippocampal neurons: implications of dermatan sulfate in neuritogenesis in the brain. *J Biol Chem* 278: 43744–43754.
- Hiraoka N, Nakagawa H, Ong E, Akama TO, Fukuda MN, Fukuda M (2000) Molecular cloning and expression of two distinct human chondroitin-4-O-sulfotransferases that belong to the HNK-1 sulfotransferase gene family. *J Biol Chem* 275: 20188–20196.
- Hiraoka N, Misra A, Belot F, Hindsaul O, Fukuda M (2001) Molecular cloning and expression of two distinct human N-acetylgalactosamine-4-O-sulfotransferases that transfer sulfate to GalNAc beta 1->4GlcNAc beta 1->R in both N- and O-glycans. *Glycobiology* 11: 495–504.
- Hoffmann K (2007) Investigation of the HNK1 sulfotransferase family members in wild type C57Bl/6 mice. Bachelor thesis.
- Hooper LV, Manzella SM, Baenziger JU (1996) From legumes to leukocytes: biological roles for sulfated carbohydrates. *FASEB J* 10: 1137–1146.
- Howard and Reed (1998) Unbiased stereology – three dimensional measurement in microscopy. Oxford: BIOS Scientific Publications.

7. REFERENCES

- Imai Y, Kohsaka S (2002) Intracellular signaling in M-CSF-induced microglia activation: role of Iba1. *Glia* 40: 164–174.
- Inaba Y, Ichikawa M, Koh CS, Inoue A, Itoh M, Kyogashima M, Komiyama A (1999) Suppression of experimental autoimmune encephalomyelitis by dermatan sulfate. *Cell Immunol* 198: 96–102.
- Iozzo RV (1998) Matrix proteoglycans: from molecular design to cellular function. *Annu Rev Biochem* 67: 609–652.
- Irintchev A, Rollenhagen A, Tronscoso E, Kiss JZ, Schachner M (2005) Structural and functional aberrations in the cerebral cortex of tenascin-C deficient mice. *Cereb Cortex* 21: 391–402.
- Janecke AR, Unsinn K, Kreczy A, Baldissera I, Gassner I, Neu N, Utermann G, Muller T (2001) Adducted thumb-club foot syndrome in sibs of a consanguineous Austrian family. *J Med Genet* 38: 265–269.
- Kang HG, Evers MR, Xia G, Baenziger ZU, Schachner M (2001) Molecular cloning and expression of an N-acetylgalactosamine-4-O-sulfotransferase that transfers sulfate to terminal and non-terminal beta 1,4-linked N-acetylgalactosamine. *J Biol Chem* 276, 10861–10869.
- Kang HG, Evers MR, Xia G, Baenzinger JU, Schachner M (2002) Molecular cloning and characterization of chondroitin-4-O-sulfotransferase-3. A novel member of the HNK-1 family of sulfotransferases. *J Biol Chem* 277: 34766–34772.
- Kawaguchi Y, Katsumaru H, Kosaka T, Heizmann CW, Hama K (1987) Fast spiking cells in the rat hippocampus (CA1 region) contain the calcium-binding protein parvalbumin. *Brain Res* 416: 369–374.
- Kesner RP (2007) Behavioral functions of the CA3 subregion of the hippocampus. *Learn Mem* 14: 771–781.
- Kim C, Goldberger O, Gallo R, Bernfield M (1994) Members of the syndecan family of heparan sulfate proteoglycans are expressed in distinct cell-, tissue-, development-specific patterns. *Mol Biol Cell* 5: 797–805.
- Kinsella MG, Wight TN (1986) Modulation of sulfated proteoglycan synthesis by bovine aortic endothelial cells during migration. *J Biol Chem* 261: 679–687.
- Kosaka T, Katsumaru H, Hama K, Wu JY, Heizmann CW (1987) GABAergic neurons containing the Ca²⁺-binding protein parvalbumin in the rat hippocampus and dentate gyrus. *Brain Res* 419: 119–130.

7. REFERENCES

- Kosho T, Miyake N, Hatamochi A, Takahashi J, Kato H, Miyahara T, Igawa Y, Yasui H, Ishida T, Ono K, Kosuda T, Inoue A, Kohyama M, Hattori T, Ohashi H, Nishimura G, Kawamura R, Wakui K, Fukushima Y, Matsumoto N (2010) A new Ehlers-Danlos syndrome with craniofacial characteristics, multiple congenital contractures, progressive joint and skin laxity, and multisystem fragility-related manifestations. *Am J Med Genet A* 152A: 1333–1346.
- Kosho T, Takahashi J, Ohashi H, Nishimura G, Kato H, Fukushima Y (2005) Ehlers-Danlos syndrome type VIB with characteristic facies, decreased curvatures of the spinal column, and joint contractures in two unrelated girls. *Am J Med Genet A* 138A: 282–287.
- Lafont F, Rouget M, Triller A, Prochiantz A, Rousselet A (1992) In vitro control of neuronal polarity by glycosaminoglycans. *Development* 114: 17–29.
- Leteux C, Chai W, Loveless RW, Yuen CT, Uhlin-Hansen L, Combarnous Y, Jankovic M, Maric SC, Misulovin Z, Nussenzweig MC, Feizi T (2000) The cysteine-rich domain of the macrophage mannose receptor is a multispecific lectin that recognizes chondroitin sulfates A and B and sulfated oligosaccharides of blood group Lewis(a) and Lewis(x) types in addition to the sulfated N-glycans of lutropin. *J Exp Med* 191: 1117–11126.
- Leuner B, Gould E (2010) Structural plasticity and hippocampal function. *Annu Rev Psychol* 61: 111–40.
- Liaw PC, Becker DL, Stafford AR, Fredenburgh JC, Weitz JI (2001) Molecular basis for the susceptibility of fibrin-bound thrombin to inactivation by heparin cofactor ii in the presence of dermatan sulfate but not heparin. *J Biol Chem* 276: 20959–20965.
- Löffler G, Petrides PE, Heinrich PC (2007) Springer-Lehrbuch Biochemie und Pathobiochemie, 8. völlig neu bearbeitete Auflage: 30.
- Lyon M, Deakin JA, Rahmoune H, Fernig DG, Nakamura T, Gallagher JT (1998) Hepatocyte growth factor/scatter factor binds with high affinity to dermatan sulfate. *J Biol Chem* 273: 271–278.
- Maccaferri G, Roberts JD, Szucs P, Cottingham CA, Somogyi P (2000) Cell surface domain specific postsynaptic currents evoked by identified GABAergic neurones in rat hippocampus in vitro. *J Physiol (Lond)* 524: 91–116.
- Maccarana M, Olander B, Malmström J, Tiedemann K, Aebersold R, Lindahl U, Li JP, Malmström A (2006) Biosynthesis of dermatan sulfate: chondroitin-glucuronate C5-epimerase is identical to SART2. *J Biol Chem* 281:11560-8.
- Maimone MM, Tollefsen DM (1990) Structure of a dermatan sulfate hexasaccharide that binds to heparin cofactor II with high affinity. *J Biol Chem* 265: 18263-71.

7. REFERENCES

- Malfait F, Syx D, Vlummens P, Symoens S, Nampoothiri S, Hermanns-Lê T, Van Laer L, De Paepe A (2010) Musculocontractural Ehlers-Danlos Syndrome (former EDS type VIB) and adducted thumb clubfoot syndrome (ATCS) represent a single clinical entity caused by mutations in the dermatan-4-sulfotransferase 1 encoding CHST14 gene. *Hum Mutat* 31: 1233-9.
- Malmström A (1984) Biosynthesis of dermatan sulfate. II. Substrate specificity of the C-5 uronosyl epimerase. *J Biol Chem* 259: 161–165.
- Mikami T, Mizumoto S, Kago N, Kitagawa H, Sugahara K (2003) Specificities of three distinct human chondroitin/dermatan N-acetylgalactosamine, 4-O-sulfotransferases demonstrated using partially desulfated dermatan sulfate as an acceptor: implication of differential roles in dermatan sulfate biosynthesis. *J Biol Chem* 278: 36115–36127.
- Mitsunaga C, Mikami T, Mizumoto S, Fukuda J, Sugahara K (2006) Chondroitin sulfate/dermatan sulfate hybrid chains in the development of cerebellum. Spatiotemporal regulation of the expression of critical disulfated disaccharides by specific sulfotransferases. *J Biol Chem* 281: 18942–18952.
- Moran LB, Graeber MB (2004) The facial nerve axotomy model. *Brain Res Rev* 44: 154–178.
- Morellini F, Sivukhina E, Stoenica L, Oulianova E, Bukalo O, Jakovcevski I, Dityatev A, Irintchev A, Schachner M (2010) Improved reversal learning and working memory and enhanced reactivity to novelty in mice with enhanced GABAergic innervation in the dentate gyrus. *Cereb Cortex* 11: 2712–27.
- Miyake N, Kosho T, Mizumoto S, Furuichi T, Hatamochi A, Nagashima Y, Arai E, Takahashi K, Kawamura R, Wakui K, Takahashi J, Kato H, Yasui H, Ishida T, Ohashi H, Nishimura G, Shiina M, Saitsu H, Tsurusaki Y, Doi H, Fukushima Y, Ikegawa S, Yamada S, Sugahara K, Matsumoto N (2010) Loss-of-function mutations of CHST14 in a new type of Ehlers-Danlos syndrome. *Hum Mutat* 31: 966-74.
- Nadanaka S, Fujita M, Sugahara K (1999) Demonstration of a novel sulfotransferase in fetal bovine serum, which transfers sulfate to the C6 position of the GalNAc residue in the sequence iduronic acid alpha1-3GalNAc beta1-4iduronic acid in dermatan sulfate. *FEBS Lett* 452: 185–189.
- Nickel S (2009) Analyse der CHST-14 Knockout-Maus (*Mus musculus*, Linné 1758). Doctoral thesis, University of Hamburg, Hamburg, Germany.
- Nikonenko AG, Sun M, Lepsveridze E, Apostolova I, Petrova I, Irintchev A, Dityatev A, Schachner M (2006) Enhanced perisomatic inhibition and impaired long-term potentiation in the CA1 region of juvenile CHL1-deficient mice. *Eur J Neurosci* 23: 1839–1852.

7. REFERENCES

- Ong E, Yeh JC, Ding Y, Hindsgaul O, Pedersen LC, Negishi M, Fukuda M (1999) Structure and function of HNK-1 sulfotransferase. Identification of donor and acceptor binding sites by site-directed mutagenesis. *J Biol Chem* 274: 25608–25612
- Pacheco B, Maccarana M, Malmström A (2009b) Dermatan 4-O-sulfotransferase 1 is pivotal in the formation of iduronic acid blocks in dermatan sulfate. *Glycobiology* 19: 1197–1203.
- Pacheco B, Malmström A, Maccarana M (2009a). Two dermatan sulfate epimerases form iduronic acid domains in dermatan sulfate. *J Biol Chem* 284: 9788–9795.
- Penc SF, Pomahac B, Winkler T, Dorschner RA, Eriksson E, Herndon M, Gallo RL (1998) Dermatan sulfate released after injury is a potent promoter of fibroblast growth factor-2 function. *J Biol Chem* 273: 28116–28121.
- Penc SF, Pomahac B, Eriksson E, Detmar M, Gallo RL (1999) Dermatan sulfate activates nuclear factor-kappaB and induces endothelial and circulating intercellular adhesion molecule-1. *J Clin Invest* 103: 1329–1335.
- Pesold C, Liu WS, Guidotti A, Costa E, Caruncho HJ (1999) Cortical bitufted, horizontal, and Martinotti cells preferentially express and secrete reelin into perineuronal nets, nonsynaptically modulating gene expression. *Proc Natl Acad Sci USA* 96: 3217–3222.
- Rickmann M, Wolff JR (1995) Modifications of S-100-protein immunoreactivity in rat brain induced by tissue preparation. *Histochem Cell Biol* 103: 135–145.
- Rosenberg LC, Choi HU, Tang LH, Johnson TL, Pal S, Webber C, Reiner A, Poole AR (1985) Isolation of dermatan sulfate proteoglycans from mature bovine articular cartilages. *J Biol Chem* 260: 6304–6313.
- Rostand KS, Esko JD (1997) Microbial adherence to and invasion through proteoglycans. *Infect Immun* 65: 1–8.
- Schmidtchen A, Frick I, Björck L (2001) Dermatan sulphate is released by proteinases of common pathogenic bacteria and inactivates anticacterial alpha-defensin. *Mol Microbiol* 39: 708–713.
- Schmitz B, Schachner M, Ito Y, Nakano T, Ogawa T (1994) Determination of structural elements of the L2/HNK-1 carbohydrate epitope required for its function. *Glycoconj J* 11: 345–352.
- Sidman RL, Angevine JB, Pierce ET (1971) *Atlas of the Mouse Brain and Spinal Cord*. Harvard Univ Press.
- Silbert JE, Sugumaran G (2002a) A starting place for the road to function. *Glycoconj J* 19: 227–237.

7. REFERENCES

Silbert JE, Sugumaran G (2002b) Biosynthesis of chondroitin/dermatan sulfate. *IUBMB Life* 54: 177–186.

Silbert JE, Palmer ME, Humphries DE, Silbert CK (1986) Formation of dermatan sulfate by cultured human skin fibroblasts. Effects of sulfate concentration on proportions of dermatan/chondroitin. *J Biol Chem* 261: 13397–13400.

Sofroniew MV, Schrell U (1982) Long-term storage and regular repeated use of diluted antisera in glass staining jars for increased sensitivity, reproducibility, and convenience of single- and two-color light microscopic immunocytochemistry. *J Histochem Cytochem* 30: 504–511.

Somogyi P, Klausberger T (2005) Defined types of cortical interneurone structure space and spike timing in the hippocampus. *J Physiol* 562: 9–26.

Steinmann B, Gitzelmann R, Vogel A, Grant ME, Harwood R, Sear CH. (1975) Ehlers-Danlos syndrome in two siblings with deficient lysyl hydroxylase activity in cultured skin fibroblasts but only mild hydroxylysine deficit in skin. *Helv Paediatr Acta* 30: 255–274.

Steinmann B, Royce PM, Superti-Furga A (2002) The Ehlers-Danlos syndrome. In: Royce PM, Steinmann B, editors. *Connective tissue and heritable disorders*. Hoboken, NJ: John Wiley & Sons Inc. p 431–523.

Sonoda T, Kouno K (2000) Two brothers with distal arthrogryposis, peculiar facial appearance, cleft palate, short stature, hydronephrosis, retentio testis, and normal intelligence: A new type of distal arthrogryposis? *Am J Med Genet* 91: 280–285.

Streit WJ, Walter SA, Pennell NA (1999) Reactive microgliosis. *Prog Neurobiol* 57: 563–581.

Sugahara K, Kitagawa H (2000) Recent advances in the study of the biosynthesis and functions of sulfated glycosaminoglycans. *Curr Opin Struct Biol* 10: 518–527.

Sugahara K, Mikami T, Uyama T, Mizuguchi S, Nomura K, Kitagawa H (2003) Recent advances in the structural biology of chondroitin sulfate and dermatan sulfate. *Curr Opin Struct Biol* 13: 612–620.

Szabadics J, Lorincz A, Tamas G (2001) β and γ frequency synchronization by dendritic GABAergic synapses and gap junctions in a network of cortical interneurons. *J Neurosci* 21: 5824–5831.

Tamas G, Buhl EH, Lorincz A, Somogyi P (2000) Proximally targeted GABAergic synapses and gap junctions synchronize cortical interneurons. *Nat Neurosci* 3: 366–371.

7. REFERENCES

Taylor KR, Rudisill JA, Gallo RL (2005) Structural and sequence motifs in dermatan sulfate for promoting fibroblast growth factor-2 (FGF-2) and FGF-7 activity. *J Biol Chem* 280: 5300–5306.

Trowbridge JM, Rudisill JA, Ron D, Gallo RL (2002) Dermatan sulfate binds and potentiates activity of keratinocyte growth factor (FGF-7). *J Biol Chem* 277: 42815–42820.

Trowbridge JM, Gallo RL (2002) Dermatan sulfate: new functions from an old glycosaminoglycan. *Glycobiology* 12: 117R–125R.

Walker LC, Overstreet MA, Willing MC, Marini JC, Cabral WA, Pals G, Bristow J, Atsawasuwan P, Yamauchi M, Yeowell HN. (2004) Heterogeneous basis of the type VIB form of Ehlers-Danlos syndrome (EDS VIB) that is unrelated to decreased collagen lysyl hydroxylation. *Am J Med Genet A* 131:155–162.

Wolf HK, Buslei R, Schmidt-Kastner R, Schmidt-Kastner PK, Pietsch T, Wiestler OD, Bluhmke I (1996) NeuN: a useful neuronal marker for diagnostic histopathology. *J Histochem Cytochem* 44: 1167–1171.

Wrenshall LE, Stevens RB, Cerra FB, Platt JL (1999) Modulation of macrophage and B cell function by glycosaminoglycans. *J Leukoc Biol* 66: 391–400.

Xia G, Evers MR, Kang HG, Schachner M, Baenziger JU (2000) Molecular cloning and expression of the pituitary glycoprotein hormone N-acetylgalactosamine 4-O-sulfotransferases. *J Biol Chem* 275: 38402–38409.

Yamaguchi Y, Mann DM, Ruoslahti E (1990) Negative regulation of transforming growth factor-beta by the proteoglycan decorin. *Nature* 346: 281–284.

Yeowell H, Steinmann B (2000) Ehlers-Danlos syndrome, kyphoscoliotic form. Seattle, WA: University of Washington.

Ylinen A, Bragin A, Nadasdy Z, Jando G, Szabo I, Sik A, Buzsaki G (1995) Sharp wave-associated high-frequency oscillation (200 Hz) in the intact hippocampus: network and intracellular mechanisms. *J Neurosci* 15: 30–46.

8. ABBREVIATIONS

%	Percent
°C	Degrees Celsius
μ	Micro (10 ⁻⁶)
3`-PB	3`-phosphosulfonate binding site
5`-PSB	5`-phosphosulfonate binding site
ATCS	Adducted thumb-clubfoot syndrome
C4ST1	Chondroitin-4O-sulfotransferase1
C4ST2	Chondroitin-4O-sulfotransferase2
C4ST3	Chondroitin-4O-sulfotransferase3
CA1	Region in the hippocampus
CA3	Region in the hippocampus
CaCl ₂	Calcium chloride
CCK	Cholecystokinin
cDNA	Complementary desoxyribonucleic acid
CHL1	Close homologue of L1
Chst8	N-acetylgalactosamine-4O-sulfotransferase 1
Chst9	N-acetylgalactosamine-4O-sulfotransferase 2
Chst10	Chondroitin sulfotransferase 10
Chst11	Chondroitin-4O-sulfotransferase 1
Chst12	Chondroitin-4O-sulfotransferase 2
Chst13	Chondroitin-4O-sulfotransferase 3
Chst14	Dermatan-4O-sulfotransferase1
Chst14 -/-	Chst14 deficient
Chst14 +/-	Chst14 non-deficient
CNPase	2',3'-cyclic nucleotide 3'-phosphodiesterase
CNS	Central nervous system
CS	Chondroitin sulfate
CS B	Chondroitin sulfate B
Cy2	Cyanine 2
Cy3	Cyanine 3
D4ST1	Dermatan-4O-sulfotransferase1
DG	Gyrus dentatus

8. ABBREVIATIONS

DS	Dermatan sulfate
e.g.	exempli gratia (for example)
ECM	Extracellular matrix
EDS	Ehlers-Danlos syndrome
Fig.	Figure
g	Gram
GABA	Gamma amino butyric acid
GAG(s)	Glycosaminoglycan(s)
GalNAc	N-acetylgalactosamine
GalNAc4ST1	N-acetylgalactosamine-4O-sulfotransferase1
GalNAc4ST2	N-acetylgalactosamine-4O-sulfotransferase2
GlcUA	Glucuronic acid
HNK-1	Human natural killer cell antigen-1
HNK-1ST	HNK-1 sulfotransferase
HS	Heparan sulfate
hu	Human
i.e.	id est (that is)
i.p.	intra peritoneal
Iba1	ionized calcium-binding adaptor molecule
IdoUA	Iduronic acid
Ig	Immunoglobulin
kDa	Kilo Dalton
KS	Keratin sulfate
l	Litre
M	Molar
mg	Miligram
ml	Mililitre (Litre $\times 10^{-3}$)
mm	Milimetre (Metre $\times 10^{-3}$)
mM	Milimolar
NaOH	Sodium hydroxide solution
NCAM	Neural cell adhesion molecule
NeuN	Neuron specific nuclear antigen
PAPS	3'-phosphoadenosine 5'-phosphosulfate

8. ABBREVIATIONS

PBS	Phosphate Buffered Saline
PCR	Polymerase chain reaction
PG(s)	Proteoglycan(s)
pH	p(otential) of H(ydrogen), the logarithm of the reciprocal of hydrogen-ion concentration in gram atoms per litre
PV	Parvalbumin
RNA	Ribonucleic acid
RT	Room temperature
S-100	Low molecular weight calcium-binding protein expressed in astrocytes
SD	Standard difference
SEM	Standard errors of mean
SNP	Single nucleotide polymorphism
SPSS	Statistical Product and Service Solutions
ST	Sulfotransferase
TM	Transmembrane domain
v/v	Volume per volume
VGAT	Vesicular GABA transporter
w/v	Weight/volume
ZMNH	Zentrum für Molekulare Neurobiologie Hamburg

9. DANKSAGUNG

Die Durchführung dieser Dissertation erfolgte am Institut für Biosynthese neuraler Strukturen am Zentrum für molekulare Neurobiologie Hamburg (ZMNH). Frau Prof. Dr. Melitta Schachner möchte ich als Doktormutter und Direktorin des Instituts herzlich für die Überlassung des interessanten Themas, die Bereitstellung des Arbeitsplatzes und die Hilfs- und Diskussionsbereitschaft danken.

An meinen Betreuer Dr. Andrey Irintchev richtet sich mein ganz besonderer Dank. Von Beginn bis zur Fertigstellung der Arbeit erfuhr ich durch seine stets motivierende und fachkompetente Unterstützung eine hervorragende Betreuung.

Sowohl für die tatkräftige Hilfestellung, die Diskussionsbereitschaft als auch für das kritische und produktive Korrekturlesen danke ich zudem Igor Jakovcevski und Nuray Agyüz.

Bei Frau Emanuela Szpotowicz bedanke ich mich sehr herzlich für die Unterstützung beim Schneiden und Färben des Mausgewebes.

Ferner möchte ich mich auch bei den Kollegen aus dem Labor bedanken, die mir den Umgang mit dem Mikroskop erklärten und immer mit Rat und Tat zur Seite standen.

Abschließend bedanke ich mich bei meinem Freund Jan Buchartz, meinen Freunden und bei meiner Familie für ihre aufmunternde und geduldige Unterstützung.

10. CURRICULUM VITAE

Personal Data

Name: Ewa Helena Laczynska

Date of Birth: August 5th 1982

Place of Birth: Danzig / Poland

Nationality: Polish / German

Professional Experience

since 02/2011 Specialized training in Paediatrics
Department of Neonatology at the Bürgerhospital, Frankfurt am Main
Neonatal Intensive Care Unit

05/2009 – 01/2011 Specialized training in Paediatrics
Children`s hospital at the Klinikum Offenbach, Offenbach

Infectious disease ward; newborn and infant ward; general paediatrics ward;
emergency outpatient clinic

Education

02/2009 License to practice medicine

10/2002 – 12/2008 Studies of Medicine at the University of Hamburg

09/1993-06/2002 Bremen General Abitur (qualification for university)

Dissertation (since 05/2006)

Stereological Analysis of the Motor Cortex and the Hippocampus of Dermatan-4O-sulfotransferase1 (Chondroitin Sulfotransferase 14) knockout mice.

Department of biosynthesis of neural structures at the center for molecular neurobiology
Hamburg (ZMNH), Director Prof. Dr. M. Schachner

11. EIDESSTATTLICHE VERSICHERUNG

Ich versichere ausdrücklich, dass ich die Arbeit selbständig und ohne fremde Hilfe verfasst, andere als die von mir angegebenen Quellen und Hilfsmittel nicht benutzt und die aus den benutzten Werken wörtlich oder inhaltlich entnommenen Stellen einzeln nach Ausgabe (Auflage und Jahr des Erscheinens), Band und Seite des benutzten Werkes kenntlich gemacht habe.

Ferner versichere ich, dass ich die Dissertation bisher nicht einem Fachvertreter an einer anderen Hochschule zur Überprüfung vorgelegt oder mich anderweitig um Zulassung zur Promotion beworben habe.

Ewa Helena Laczynska